Ore Geology Reviews 90 (2017) 307–321

Contents lists available at ScienceDirect

Ore Geology Reviews

journal homepage: www.elsevier.com/locate/oregeo

Chromite compositions in nickel sulphide mineralized intrusions of the Kabanga-Musongati-Kapalagulu Alignment, East Africa: Petrologic and exploration significance

David M. Evans *

Department of Earth Sciences, Natural History Museum, Cromwell Road, London SW7 5BD, United Kingdom

ARTICLE INFO

Article history:
Received 27 July 2016
Received in revised form 1 March 2017
Accepted 10 March 2017
Available online 14 March 2017

Keywords:
Kibaran
Nickel sulphide
Chromite
Magma contamination
Sulphur saturation
Oxygen fugacity

ABSTRACT

Chromite is a ubiquitous accessory mineral in the olivine-pyroxene cumulate bodies that host massive and disseminated nickel sulphide mineralization in intrusions of the Kabanga-Musongati-Kapalagulu Alignment in East Africa. Its composition is related to the conditions of emplacement and petrologic evolution of its host magma in a spectrum of intrusions ranging from classical lopolithic layered intrusions to groups of smaller, discrete sill-like chonoliths.

The Kapalagulu lopolithic intrusion, emplaced into polymetamorphosed Archæan-Palæoproterozoic crust, contains abundant chromite with relatively oxidized compositions, whereas chromites from the highly-mineralized Kabanga chonolith intrusions, emplaced into graphitic and sulphidic schists, are strongly reduced in terms of their Fe^{3+}/Fe^{total} ratio. Ni in chromite correlates with Ni in olivine: Ni in both is depleted in the more strongly sulphide-mineralized intrusions. The Musongati intrusion, also emplaced through graphitic schists, but much larger and less-well mineralized in sulphides than Kabanga, has chromites intermediate in character. The compositions of the chromites can be used to determine the petrologic history of the intrusions, and may prove to be a useful exploration tool in such mineralized belts.

1. Introduction

The East African Nickel Belt is a newly defined large mineralized province, which has the potential to become the most important nickel producing region in Africa (Evans et al., 2016). A large and high-grade, but as yet unexploited, resource of magmatic nickel sulphides is indicated in the Kabanga intrusions of northwestern Tanzania (Fig. 1), and large lateritic nickel deposits exist at Musongati in Burundi (Deblond and Tack, 1999) and at Kapalagulu in western Tanzania (Wilhelmij and Cabri, 2015). Both the sulphide and lateritic nickel deposits are hosted by or derived from mafic-ultramafic intrusive rocks of the Mesoproterozoic Kibaran tectonothermal province (Tack et al., 2010).

Most of the mafic-ultramafic intrusions of the Kibaran province contain some magmatic sulphides, but only a very few contain sufficient abundance of sulphides at a high enough metal tenor to be considered potentially economic (Evans et al., 2016). The larger intrusions have a lopolithic form and mainly contain weakly disseminated sulphides in their lower, ultramafic layers (Deblond and Tack, 1999). The highest abundances of Ni-Cu-bearing sulphides occur in clusters of the smaller intrusions, which have the form of subconcordant chonoliths (highly elongated, narrow sill-like differentiated bodies; Maier et al., 2010). The challenge for commercial exploration of this type of magmatic sulphide deposit is to determine which of the many geophysical and geochemical anomalies that are generated in regional exploration are related to economic mineralization.

Chromite, or more generally, chrome-spinel has been proposed as a mineral, resistant to weathering, that can preserve information in its texture and composition on the processes that led to its formation and subsequent modifications (Irvine, 1967; Dick and Bullen, 1984). It is also a common accessory in ultramafic cumulate rocks associated with magmatic nickel sulphide deposits and has the potential to differentiate between different petrologic histories and hence ore-forming processes (Barnes and Tang, 1999; Barnes and Kunilov, 2000). I propose to examine its use to unravel the evolution of the Kibaran mafic-ultramafic intrusions and provide constraints for its use in mineral exploration of this belt.

2. Geological overview

2.1. Structure and stratigraphy of the Karagwe-Ankole belt

Three of the intrusions discussed here, the Kabanga, Muremera and Musongati intrusions (Fig. 1a) occur within the Palæo- to

* Address: 21 rue Jean de la Bruyère, Versailles, 78000, France.
E-mail address: evans_dave_m@hotmail.com

http://dx.doi.org/10.1016/j.oregeorev.2017.03.012
0169-1368/

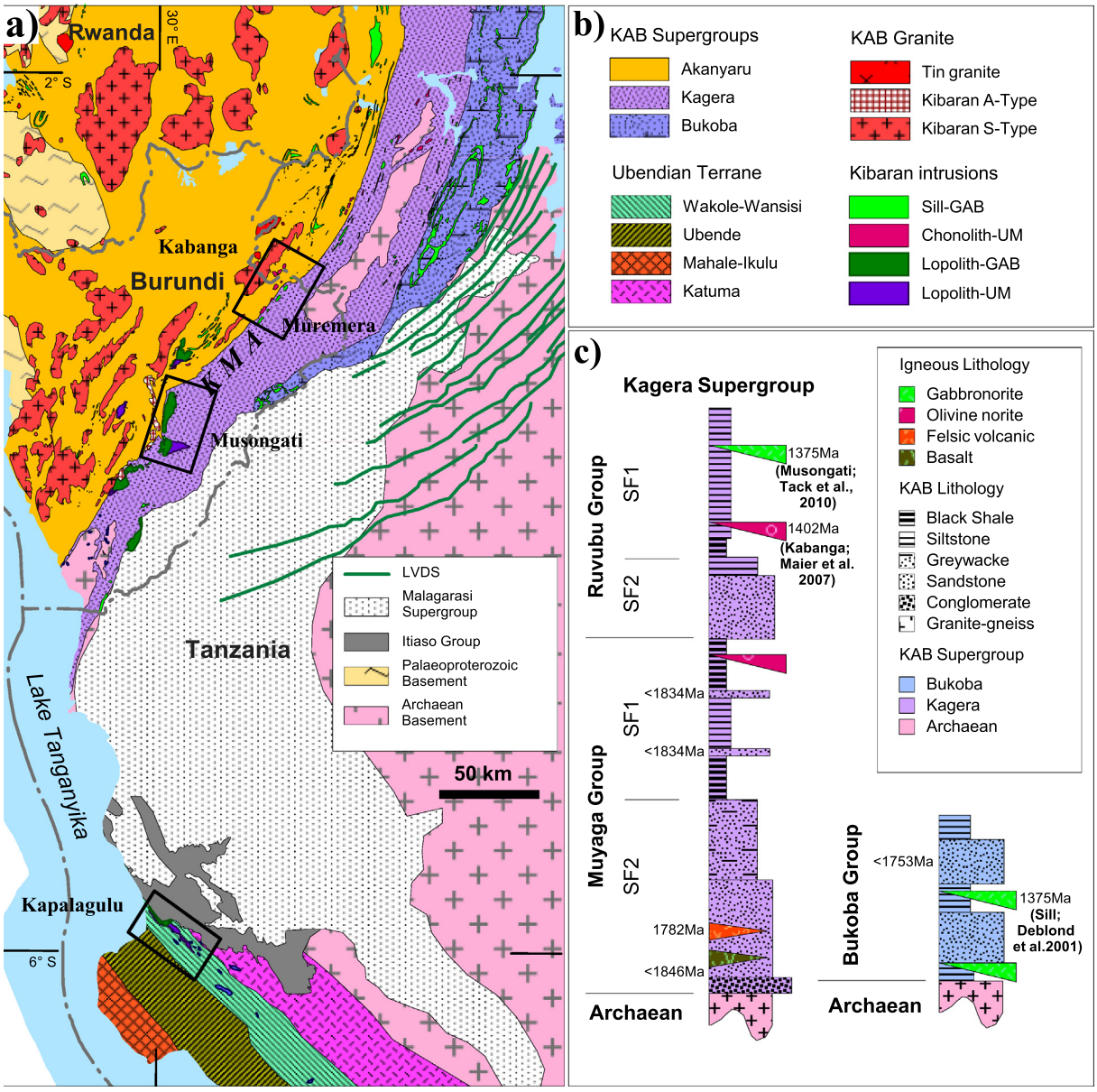

Fig. 1. a) Geological map of the East African nickel belt (modified from Tack et al., 2010) showing the localities of the Kabanga, Muremera, Musongati and Kapalagulu intrusions (boxes correspond to detailed geological plans in Fig. 2); **b)** Legend for (a); **c)** Schematic stratigraphic column for the Kagera Supergroup, modified from Fernandez-Alonso et al. (2012), and Koegelenberg et al. (2015). *Abbreviations:* GAB gabbro, UM ultramafic, SF Superformation.

Mesoproterozoic Karagwe-Ankole Belt (KAB). The KAB consists of a thick sequence of siliciclastic epicontinental to intracontinental sedimentary rocks overlying Archæan to Palæoproterozoic infracrustal basement (Fig. 1). The sedimentary rocks, which were deposited between 1.78 Ga and 1.37 Ga, include subordinate quartzites and predominant mica schists or phyllites, locally highly graphitic and sulphidic that have been moderately folded and metamorphosed during the Mesoproterozoic era (Fernandez-Alonso et al., 2012; Koegelenberg et al., 2015).

Regional mapping in eastern Burundi (Waleffe, 1966) and in Rwanda (Baudet et al., 1988) established a stratigraphic framework, while later mapping of central Burundi defined a structural-magmatic framework for the KAB (Klerkx et al., 1987; Theunissen et al., 1992; Tack et al., 1994). These frameworks were updated, modified and formalized for the whole KAB by Tack et al. (2010) and Fernandez-Alonso et al. (2012), using well-constrained modern U-Pb dating of igneous and sedimentary detrital zircons of the belt. These authors divide the KAB into two main tectonic-stratigraphic domains, the Eastern Domain and the Western Domain (after Tack et al., 1994), underlain respectively by Archæan cratonic and Palæoproterozoic orogenic crust. The sedimentary rocks of the KAB are also divided on the same basis into two separate, parallel sub-basin sequences for which the formal stratigraphic terminology Akanyaru Supergroup (Western Domain) and Kagera Supergroup (Eastern Domain) were introduced (Fernandez-Alonso et al., 2012).

In broad terms, per Fernandez-Alonso et al. (2012) and Westerhof et al. (2014), the Kagera Supergroup comprises an autochthonous sequence of continental (conglomerates, poorly-sorted sandstones) to epicontinental or shallow-marine sediments (turbidites, ripple-bedded arenitic sandstones, carbonaceous mudstones) whose deposition is constrained (Fig. 1c) to between 1782 Ma (igneous zircons in felsic tuffs near base) and 1375 Ma (intrusion of gabbroic bodies near top). The Akanyaru Supergroup comprises a tectonically-disrupted sequence of epicontinental shelf-type sediments deposited between 1800 Ma (youngest age

of abundant detrital zircons) and 1383 Ma (earliest intrusion of batholithic peraluminous or S-type granitoids).

The mafic-ultramafic intrusions that are the subject of this study have been intruded into a transitional domain between the Eastern and Western Domains (Tack et al., 1994). For simplicity, I have assumed that they are all intruded into the sedimentary sequence of the Kagera Supergroup, and this is described in more detail below.

The Kagera Supergroup is divided formally into two fining-upwards sequences, the basal Muyaga Group and the overlying Ruvubu Group (Fig. 1C; Fernandez-Alonso et al., 2012). Each Group has been subdivided into unnamed upper (SF1) and lower (SF2) Superformations. The lower SF2 of the Muyaga Group, comprising conglomerates, grits and arkosic sandstones, unconformably overlies the Archæan basement in the south. The largely continental deposits of Muyaga SF2 grade upwards through a sequence of greywackes to a thick package of finely laminated siltstones and mudstones containing abundant sulphides and carbonaceous matter (Muyaga SF1). The lower SF2 of the Ruvubu Group comprises a package of massive-bedded to weakly cross-laminated clean arenitic sandstone beds that overlie the Muyaga Group with an apparently conformable relationship. These are followed by an apparently much thicker sequence of finely-laminated siltstones to thickly-bedded sulphide-bearing mudstones (Ruvubu SF1).

A high-T, low-P metamorphism (typified by the sequence chloritoid-andalusite-cordierite-sillimanite in metapelites) is regionally present in the KAB, in both the Akanyaru and Kagera Supergroups (Tack and Deblond, 1990). It is broadly coincident with the intrusion of granitic and mafic-ultramafic bodies into the sedimentary rocks and the immediately adjacent basement. The granitic rocks are largely peraluminous 2-mica granites (S-type) that contain both foliated and unfoliated phases (Tack et al., 2010). The mafic-ultramafic suite includes widespread doleritic sills and differentiated layered intrusions within the KAB sedimentary rocks (Duchesne et al., 2004), and an important swarm of dolerite dykes intruded into Archæan crust to the east of the KAB (the Lake Victoria Dyke Swarm: Mäkitie et al., 2014). This bimodal igneous suite (to which the Kabanga, Muremera and Musongati intrusions belong), together with the high-T metamorphism has been termed the Kibaran tectonothermal event (Tack et al., 2010) and occurred between 1330 – 1400 Ma (Maier et al., 2007; Tack et al., 2010; Mäkitie et al., 2014). A later regional compressive tectonic event, which has resulted in the present upright folding pattern of the KAB either dates from the waning stages of the Kibaran tectonothermal event (1330–1250 Ma: Koegelenberg et al., 2015) or is associated with far-field stress transfer from collision events to the south in the Irumide belt (1100–1000 Ma: Fernandez-Alonso et al., 2012).

2.2. The Ubendian Belt (UB)

The Kapalagulu intrusion (Fig. 1a) occurs at the boundary between the strongly metamorphosed Ubendian Belt (UB) and a weakly deformed sequence of intracontinental sediments, comprised of the Itiaso Group and the Malagarazi Supergroup, lying on Archæan basement rocks (Tack, 1995; Deblond et al., 2001). The UB resembles the metamorphic basement to the KAB and is formed of several parallel, elongate metamorphic terranes that have undergone different depositional and tectonic histories and that are separated by narrow, deep-crustal upright shear-zones (Daly, 1988; Theunissen et al., 1992). In western Tanzania, four of these terranes crop out adjacent to Lake Tanganyika (Fig. 1a), of which the Wakole (-Wansisi) terrane is of importance here as it structurally underlies the Kapalagulu intrusion. The terranes are dominated by high-grade felsic orthogneiss or amphibolite rocks, all of which underwent metamorphism in the Palæoproterozoic with varying degrees of reworking in the Meso- and Neoproterozoic (Lenoir et al., 1994; Boniface et al., 2012).

The Wakole Terrane is principally comprised of various types of garnetiferous amphibole schists and gneisses together with kyanite-garnet-biotite schists and quartzites (McConnell, 1950). These rocks are inferred to be largely of (volcano)-sedimentary origin and to have undergone a high-pressure metamorphic event that followed a clockwise path between 1170 Ma and 1007 Ma (Boniface et al., 2014). Zircon grains recovered from a metapelite sample of the Wakole Terrane have detrital cores that possibly indicate a minimum depositional age of 1390 Ma, although their small size limits the reliability of these ages (Boniface et al., 2014).

The Kapalagulu intrusion (Fig. 2c), reliably dated at 1392 ± 26 Ma (Maier et al., 2007), and only weakly metamorphosed, is tectonically juxtaposed along its base with hornblende-plagioclase gneisses and schists of the Wakole Terrane (Halligan, 1963; Wilhelmij and Joseph, 2004). It is apparently overlain and broadly folded with low metamorphic grade metasandstones and phyllites of the Itiaso Group, thought to be broadly correlative with the Kagera Supergroup of the KAB (Halligan, 1963). The upper margin of the intrusion with the sedimentary rocks is faulted out or not exposed (Van Zyl, 1959; Wilhelmij and Joseph, 2004), however, evidence for an intrusive relationship with the Itiaso Group lies in the presence of thermally-metamorphosed phyllites and quartzites within and near the base of the Makambo structural section of the Kapalagulu intrusion (Wilhelmij and Joseph, 2004).

2.3. Nickel mineralization of the Kibaran tectonothermal province

Mineralization directly associated with the Kibaran bimodal magmatic event is mainly found in the mafic-ultramafic intrusions, specifically as magmatic nickel sulphides within the ultramafic portions of both chonoliths and lopoliths (Deblond and Tack, 1999; Evans et al., 1999). A belt of these sulphide-mineralized, ultramafic-bearing intrusions strikes northeast-southwest across the border between Burundi and northwest Tanzania, and has been named the Kabanga-Musongati Alignment (KMA; Fig. 1a) after the two major nickel deposits contained within it (Tack et al., 1994; Deblond and Tack, 1999). The Kabanga deposit is a nickel sulphide deposit, whereas Musongati is a Ni laterite deposit developed over the sulphide-bearing ultramafic lower portion of a layered intrusion. Maier et al. (2007, 2008) propose to add the Kapalagulu intrusion to this alignment (hence KMKA) as it is similar in age, structure and lithologies to Musongati (Fig. 2b and c). Kapalagulu contains both Ni laterite and Ni-Cu sulphide mineralization as well as platinum-group element (PGE) enrichments associated with chromitite seams (Wilhelmij and Cabri, 2015).

In general, the larger, lopolithic or layered intrusions such as Musongati and Kapalagulu contain only weakly disseminated magmatic sulphides (0.5–5 modal%), but these sulphides have relatively high metal tenors (Ni or Cu content in 100% sulphide) and high PGE contents. The smaller chonoliths such as at Kabanga and Muremera are more likely to contain denser concentrations of sulphides, locally up to massive proportions (80–100 modal%), but usually with low to moderate Ni and Cu tenors and low levels of PGE (Maier and Barnes, 2010; Maier et al., 2010). It is these massive sulphide bodies of moderate Ni and Cu tenor found in chonoliths of small dimensions (Fig. 2a) that are potentially economic in the Kabanga intrusions of northwestern Tanzania (Glencore, 2016; Evans et al., 2016).

Within the KMKA intrusions, the most primitive non-cumulate marginal rocks that have been identified have the composition of siliceous high-Mg basalts (12–13% MgO, 50–52% SiO_2) and the most primitive cumulate olivines have compositions of Fo_{89} to Fo_{90} (Evans et al., 2000; Maier et al., 2008, 2010). The rocks of all these intrusions have elevated ratios of Th/Yb and La/Sm compared

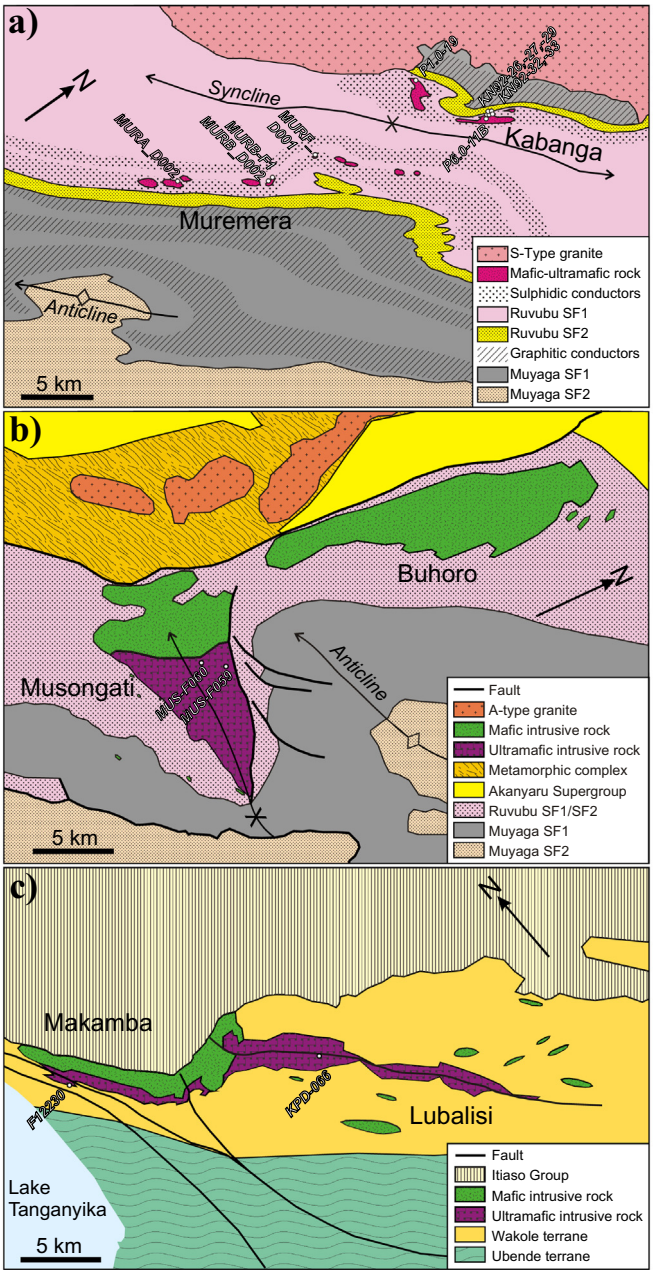

Fig. 2. Geological plans (based on national geological survey maps of Burundi and Tanzania; Wilhelmij and Cabri, 2015) of the main intrusions of the KMK alignment at the same scale, showing their inferred relations with basement and enclosing sedimentary rocks: **a)** Kabanga (north of synclinal axis) and Muremera (south of synclinal axis); **b)** Musongati; **c)** Kapalagulu. Surface locations of samples or drill holes used in the study are indicated. Conductor layers indicated in (a) are derived from surface and drill follow-up of airborne electromagnetic surveys. Abbreviations: SF Superformation.

to primitive tholeiites and picrites (Duchesne et al., 2004; Maier et al., 2008, 2010). At the Musongati, Muremera and Kabanga intrusions, the crystallization sequence is inferred to be chromite ⇒ olivine ⇒ orthopyroxene ⇒ plagioclase ⇒ clinopyroxene with orthopyroxene largely dominant over clinopyroxene and extensive orthopyroxenites developed within or near the top of the ultramafic sequence (Deblond and Tack, 1999; Evans et al., 2000). These observations, and the consistently high bulk Ni/Cu ratio of the sulphide mineralization, suggest that the parental magma was picritic in composition (14–16% MgO), but was contaminated with siliceous and CaO-poor crustal material on its way to final emplacement (Maier et al., 2010).

The Kapalagulu intrusion shows broadly similar petrological characteristics to the other KMKA intrusions, but has some important differences. The crystallization sequence is chromite ⇒ olivine ⇒ plagioclase ⇒ orthopyroxene ⇒ clinopyroxene with plagioclase chadacrysts commonly enclosed in orthopyroxene and clinopyroxene oikocrysts at the transition from the ultramafic to the mafic zone (Van Zyl, 1959; Wadsworth, 1963). Furthermore, only at Kapalagulu is chromite so abundant in the lower cumulates as to form chromitite seams (Duchesne et al., 2004; Wilhelmij and Cabri, 2015). In other respects, such as maximum Fo content of olivine and trace element ratios, the Kapalagulu cumulate rocks are similar to those of Musongati and Kabanga (Maier et al., 2008).

The crustal contamination inferred above could well have led to the saturation of the magma in sulphur, a crucial stage in the generation of magmatic Ni-Cu sulphide deposits (Naldrett, 2004; Keays and Lightfoot, 2010). Maier et al. (2008, 2010) found evidence in whole-rock geochemistry and stable isotope studies that both weakly-mineralized large lopoliths and richly-mineralized small chonoliths formed from contaminated magma, but that the magma of the small chonoliths shows higher degrees of contamination, which comes from a wider range of contaminant materials, including local host metasediments. Maier et al. (2010) also indicated that chromites in the Kabanga intrusions are relatively reduced, possibly due to contamination of parental magmas by graphitic sediments.

3. Research methodology

3.1. Sampling and petrography

Samples of typical mesocumulate and orthocumulate ultramafic rocks from unweathered surface outcrops or drill cores that have suffered minimal hydrous alteration or deformation were chosen for petrographical study of their chromites, from the Kabanga, Muremera, Musongati and Kapalagulu intrusions (locations in Fig. 2). Polished thin sections were made from these samples, which were examined by both transmitted and reflected light microscopy for identification of suitable sites for analysis at the Natural History Museum, London. Examples of the textures and mineralogy of some of these samples are shown in Fig. 3. Care was taken to avoid using samples in which higher temperature alteration has occurred (due to proximity to faults), or whose chromites show evidence of growth of ferritchromite alteration rims (Barnes, 2000; Evans, 2014).

3.2. Electron probe microanalysis

Mineral analyses were carried out at the Earth Sciences Department of the Natural History Museum, London. Chromite and some silicates were analysed by wavelength-dispersive X-ray emission spectrometry on a Cameca SX100 electron probe microanalyser (EPMA), using silicates and oxides of the major elements and pure metals for trace elements as standards. Beam current was 20 nA with an accelerating voltage of 20 kV. Major elements were counted for 15 or 20 s on the peak and for 10 s on the background. Trace elements were counted for 30 or 40 s on the peak and 20 s on the background. Raw counts were corrected for matrix absorption and fluorescence using internal Cameca software and converted to weight percent oxides, assuming all Fe as Fe^{2+}. X-ray peak overlaps of Ti Kβ on V Kα and of Fe Kβ on Co Kα were corrected for by analysis of V and Co-free Ti and Fe standards and subtraction of their relative signals from all unknown analyses. Spinel analyses were then recalculated in a spreadsheet assuming AB_2O_4 spinel stoi-

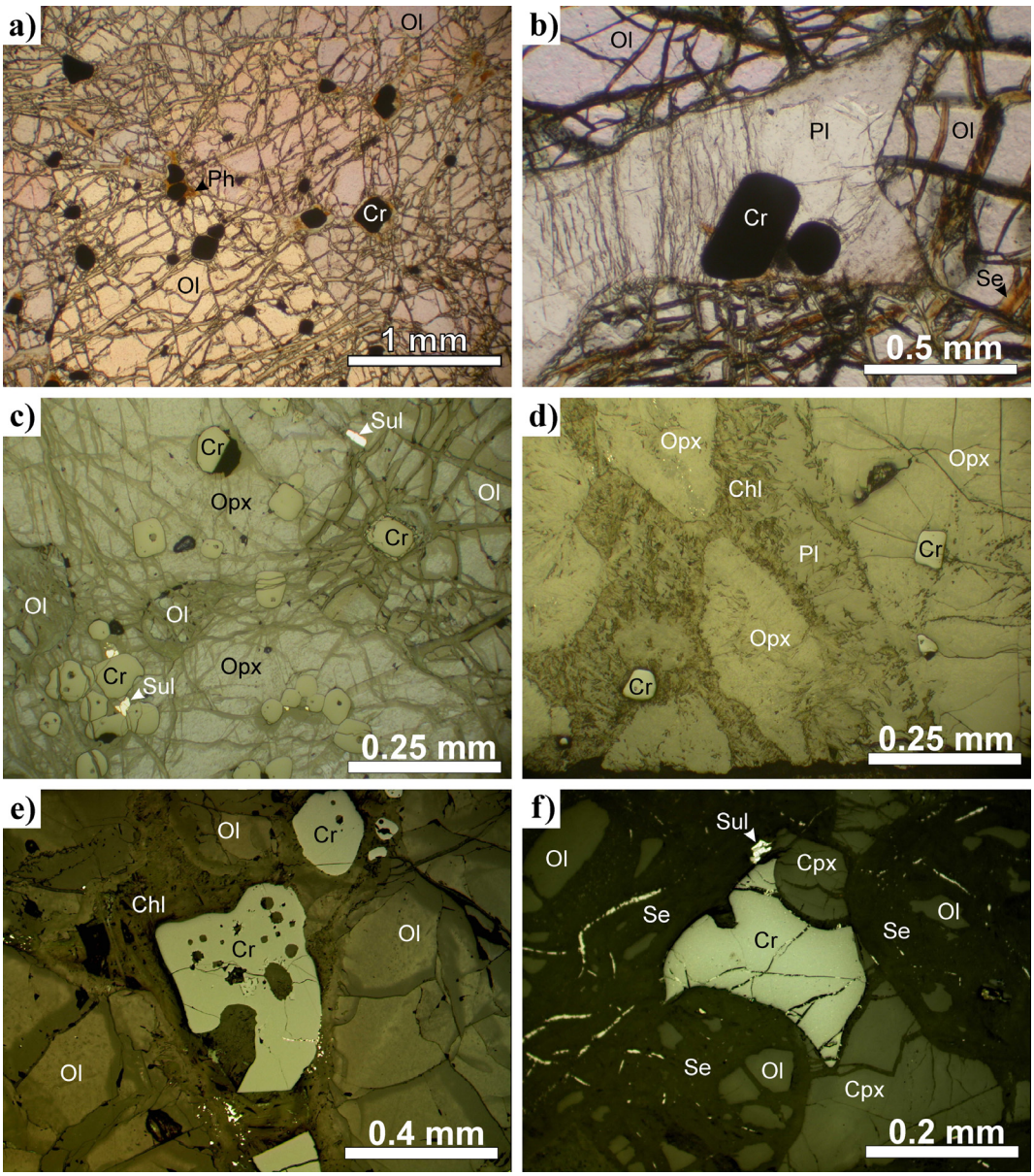

Fig. 3. Photomicrographs of chrome-spinel textures of the KMKA intrusions: **a)** subhedral chromite (type A1) within and interstitial to olivine, dunite, F12245, Kapalagulu, plane-polarized light; **b)** medium-grained subhedral chromite (type A1) within plagioclase, feldspathic harzburgite, MUS-F060-157m, Musongati, plane-polarized light; **c)** fine-grained euhedral to subhedral chromite (type A1) enclosed with reacted olivine in oikocrystic orthopyroxene, MURF_D001-80.72m, Muremera, reflected light; **d)** fine-grained euhedral chromite (type A1) enclosed in cumulate orthopyroxene and interstitial plagioclase (altered to chlorite), MURF_D001-112m, Muremera, reflected light; **e)** coarse subhedral chromite (type A2) interstitial to cumulus olivine, feldspathic lherzolite, P1.0-19-506m, reflected light; **f)** coarse anhedral chromite (type A2) interstitial with clinopyroxene between rounded olivine grains, feldspathic lherzolite, KN92-33-265m, reflected light. Mineral abbreviations: Chl chlorite mesostasis, Cpx clinopyroxene, Cr chrome-spinel, Ol olivine, Opx orthopyroxene, Ph phlogopite, Pl plagioclase, Se serpentine, Sul sulphide.

chiometry and with all TiO_2 in the ulvöspinel structure to estimate Fe^{3+}/Fe^{total} ratios (Carmichael, 1967).

To check these calculated values of Fe^{3+}/Fe^{total} ratios, secondary chromite standards that have had their Fe^{3+}/Fe^{total} ratios measured independently by Mössbauer spectroscopy were analysed during some of the analysis batches (Electronic supplementary material Table S3). It was found that corrections to Fe^{3+} due to varying Cr/Al ratios of the spinels as suggested by Wood and Virgo (1989) and Ionov and Wood (1992) were negligible. In the chromites of the KMKA, a greater source of imprecision and inaccuracy for estimation of Fe^{3+}/Fe^{total} ratios is probably the TiO_2 content. This can be quite variable even within individual grains, due to oxidation exsolution of very fine ilmenite lamellæ in those spinels with relatively high TiO_2 contents. To reduce this potential error and imprecision, several spot analyses were taken and averaged on those grains with high TiO_2 contents (>1 wt%), and those spot analyses with very high TiO_2 (>5 wt%) likely to be due to positioning of the beam over an ilmenite lamella, were omitted from this average. Cryptic zoning was noted in the chromites from Kabanga and Muremera, but chromites of Kapalagulu and Musongati were essentially homogeneous. All analyses presented here are of cores and exclude smaller grains (<30 μm). Representative analyses of chromites from the Kabanga and Muremera intrusions are given in Table 1, and from the Musongati and Kapalagulu intrusions in Table 2. Full results of all chrome-spinel analyses are given in the Electronic supplementary material Table S4.

Table 1
Representative analyses of chromites from Kabanga and Muremera intrusions.

Intrusion	Kab.	Kab.	Kab.	Kab.	Kab.	Kab.	Kab.	Kab.	Kab.	Kab.	Kab.	Kab.	Kab.	Kab.	Mur.	Mur.	Mur.	Mur.	Mur.	Mur.	Mur.	Mur.	Mur.
Sample	KB01	KB01	KB01	KB02	KB02	KB02	KB03	KB03	KB03	KB03	KB04	KB04	KB04	KB04	MR01	MR01	MR01	MR02	MR02	MR02	MR03	MR03	MR03
Host minl.	Oliv	Plag	Plag	Opx	Opx	Plag	Cpx	Opx	Oliv	Plag	Cpx	Opx	Oliv	Plag	Opx	Oliv	Plag	Cpx	Opx	Oliv	Opx	Oliv	Plag
Size μm	105	185	220	160	85	215	85	65	95	90	180	100	88	350	290	60	100	90	125	160	230	120	340
Weight % Oxides																							
MgO	7.39	9.63	11.13	9.20	12.29	7.99	10.42	11.31	7.93	8.32	9.72	13.02	8.22	9.11	9.10	5.62	4.57	8.03	10.97	6.00	12.42	4.18	9.96
Al_2O_3	18.65	16.86	19.39	16.64	20.75	16.47	22.69	24.29	22.07	25.53	22.28	23.35	23.19	24.87	19.36	21.95	19.93	17.95	20.95	18.87	20.96	18.00	22.22
SiO_2	0.058	0.047	0.086	0.064	0.092	0.068	0.049	0.049	0.034	0.171	0.049	0.036	0.036	0.073	0.074	0.094	0.036	0.028	0.154	0.013	0.056	0.034	0.035
CaO	0.000	0.006	0.007	0.000	0.004	0.006	0.000	0.000	0.000	0.094	0.004	0.006	0.000	0.011	0.001	0.004	0.014	0.000	0.014	0.000	0.004	0.000	0.029
TiO_2	0.567	1.231	1.460	0.467	0.589	0.494	1.935	0.595	2.138	1.263	0.696	0.405	0.806	0.757	0.417	1.897	2.497	3.963	0.777	0.812	0.400	1.975	0.773
V_2O_3	0.505	0.462	0.427	0.397	0.549	0.415	0.658	0.505	0.718	0.677	0.349	0.357	0.437	0.380	0.408	0.463	0.485	0.572	0.438	0.465	0.481	0.714	0.583
Cr_2O_3	47.88	50.18	47.84	51.44	48.86	51.17	43.71	45.02	41.88	40.58	44.47	45.60	41.49	41.82	48.32	38.95	40.57	41.96	45.49	43.81	46.97	42.86	43.10
MnO	0.349	0.289	0.226	0.280	0.232	0.307	0.241	0.223	0.305	0.310	0.358	0.176	0.314	0.289	0.271	0.329	0.320	0.199	0.163	0.254	0.194	0.319	0.227
$Fe'''_2O_3^{calc}$	1.08	0.93	0.20	0.89	0.00	0.65	0.00	0.00	0.45	0.00	1.57	1.03	2.24	0.71	0.86	1.91	0.98	2.10	3.06	4.59	2.36	1.96	2.55
$Fe''O^{calc}$	23.86	20.85	19.12	20.70	16.91	22.57	20.95	19.07	25.06	23.67	21.11	15.97	23.46	22.59	21.41	27.84	29.49	26.30	19.75	26.64	16.69	29.71	20.77
CoO	0.064	0.051	0.045	0.051	0.022	0.048	0.051	0.029	0.046	0.038	0.038	0.018	0.047	0.048	0.014	0.047	0.025	0.000	0.000	0.000	0.024	0.045	0.021
NiO	0.022	0.074	0.070	0.025	0.013	0.010	0.017	0.022	0.015	0.000	0.000	0.000	0.009	0.005	0.000	0.000	0.000	0.043	0.028	0.011	0.009	0.008	0.008
ZnO	0.220	0.147	0.118	0.199	0.087	0.157	0.233	0.199	0.289	0.220	0.153	0.092	0.258	0.157	0.091	0.422	0.559	0.060	0.111	0.207	0.065	0.327	0.129
Total	100.64	100.75	100.11	100.35	100.40	100.35	100.95	101.30	100.92	100.88	100.81	100.06	100.51	100.83	100.33	99.53	99.47	101.21	101.91	101.68	100.62	100.14	100.41
Mg#	35.6%	45.2%	50.9%	44.2%	56.4%	38.7%	47.0%	51.4%	36.1%	38.5%	45.1%	59.2%	38.4%	41.8%	43.1%	26.5%	21.6%	35.3%	49.8%	28.6%	57.0%	20.0%	46.1%
Fe^{3+}#	1.3%	1.2%	0.2%	1.1%	0.0%	0.8%	0.0%	0.0%	0.6%	0.0%	1.9%	1.2%	2.7%	0.9%	1.1%	2.5%	1.3%	2.8%	3.7%	5.7%	2.8%	2.6%	3.1%
Cr#	63.3%	66.6%	62.3%	67.5%	61.2%	67.6%	56.4%	55.4%	56.0%	51.6%	57.2%	56.7%	54.6%	53.0%	62.6%	54.4%	57.7%	61.1%	59.3%	60.9%	60.1%	61.5%	56.6%

Kabanga samples: KB01 = KN92-33-265.0m; KB02 = KN92-26-164m; KB03 = KN92-29-198.0m; KB04 = P1.0-19-506m.
Muremera samples: MR01 = MURB-F1-40.0m; MR02 = MURF_D001-54.0m; MR03 = MURF_D001-80.7m.

Table 2
Representative analyses of chromites from Kapalagulu and Musongati intrusions.

Intrusion	Kap.	Kap.	Kap.	Kap.	Kap.	Kap.	Kap.	Kap.	Kap.	Kap.	Kap.	Kap.	Kap.	Kap.	Kap.	Mus.	Mus.	Mus.	Mus.	Mus.	Mus.	Mus.	Mus.	Mus.	Mus.
Sample	KP01	KP01	KP01	KP02	KP02	KP02	KP02	KP03	KP03	KP03	KP04	KP04	KP04	KP05	KP05	MS01	MS01	MS02	MS02	MS02	MS03	MS03	MS03	MS04	MS04
Host minl.	Oliv	Sul	Cpx	Opx	Oliv	Plag	Sul	Opx	Oliv	Plag	Opx	Oliv	Sul	Opx	Oliv	Oliv	Plag	Opx	Opx	Plag	Oliv	Plag	Phlog	Oliv	Plag
Size μm	70	200	220	220	95	120	151	152	80	125	65	80	500	100	100	95	125	90	110	300	70	200	120	90	180
Weight% Oxides																									
MgO	7.09	7.91	8.70	9.36	6.33	7.66	6.92	8.57	6.65	8.56	10.42	8.00	8.55	8.01	7.55	5.64	4.66	9.61	8.22	6.06	6.88	10.87	7.73	7.02	8.34
Al_2O_3	15.00	15.18	16.09	18.97	13.65	15.05	12.81	14.26	11.39	14.98	19.38	13.98	15.06	19.03	14.22	17.74	17.28	16.04	12.16	10.18	13.27	18.65	14.80	15.23	16.91
SiO_2	0.000	0.009	0.006	0.015	0.017	0.015	0.000	0.009	0.004	0.013	0.041	0.026	0.026	0.064	0.039	0.009	0.032	0.039	0.011	0.002	0.068	0.073	0.053	0.019	0.013
CaO	0.001	0.003	0.000	0.000	0.000	0.015	0.025	0.000	0.004	0.003	0.041	0.000	0.000	0.003	0.031	0.000	0.021	0.013	0.000	0.000	0.000	0.000	0.000	0.001	0.011
TiO_2	2.75	2.77	2.12	1.04	2.37	2.10	1.25	2.88	2.30	1.63	1.03	2.70	2.31	1.55	1.81	2.162	0.758	2.310	3.915	3.666	2.837	2.380	3.384	3.595	2.118
V_2O_3	0.350	0.365	0.332	0.334	0.391	0.353	0.355	0.381	0.324	0.331	0.293	0.315	0.312	0.281	0.318	1.327	1.046	0.400	0.541	0.521	0.537	0.378	0.538	0.477	0.497
Cr_2O_3	40.54	40.09	41.66	40.29	40.95	40.93	44.43	40.68	41.59	42.65	42.31	41.54	41.74	40.18	42.56	43.26	46.97	40.33	37.79	36.55	47.73	45.43	45.69	43.42	44.85
MnO	0.296	0.254	0.223	0.281	0.337	0.306	0.369	0.293	0.340	0.297	0.138	0.244	0.245	0.444	0.296	0.309	0.352	0.213	0.265	0.341	0.258	0.146	0.232	0.479	0.217
$Fe'''_2O_3^{calc}$	11.18	11.36	10.15	9.51	11.67	11.15	11.10	11.89	14.03	10.44	8.02	11.70	11.07	8.65	10.93	3.07	1.75	11.72	15.72	18.55	4.72	3.76	5.41	6.55	5.47
$Fe''O^{calc}$	24.18	22.85	21.74	20.61	24.68	22.80	23.36	21.61	23.74	21.21	19.42	22.58	21.90	22.83	22.73	26.16	27.12	20.33	22.11	24.84	24.10	18.98	23.59	24.48	22.42
CoO	0.019	0.006	0.006	0.041	0.036	0.058	0.032	0.031	0.037	0.029	0.008	0.023	0.000	0.023	0.000	0.045	0.069	0.003	0.001	0.010	0.029	0.022	0.015	0.018	0.017
NiO	0.095	0.106	0.087	0.087	0.087	0.107	0.076	0.117	0.126	0.106	0.067	0.108	0.070	0.221	0.173	0.046	0.034	0.207	0.213	0.228	0.112	0.106	0.108	0.070	0.060
ZnO	0.203	0.124	0.147	0.131	0.185	0.121	0.119	0.111	0.143	0.172	0.133	0.167	0.164	0.124	0.215	0.352	0.536	0.075	0.076	0.158	0.222	0.101	0.156	0.147	0.164
Total	101.71	101.02	101.27	100.66	100.71	100.66	100.86	100.83	100.69	100.41	101.30	101.39	101.44	101.40	100.87	100.12	100.64	101.29	101.02	101.11	100.76	100.90	101.71	101.51	101.09
Mg#	34.3%	38.2%	41.6%	44.7%	31.4%	37.5%	34.6%	41.4%	33.3%	41.8%	48.9%	38.7%	41.0%	38.5%	37.2%	27.8%	23.5%	45.7%	39.9%	30.3%	33.7%	50.5%	36.9%	33.8%	39.9%
Fe^{3+}#	14.5%	14.7%	12.8%	11.7%	15.3%	14.3%	14.3%	15.4%	18.6%	13.3%	9.7%	15.1%	14.1%	10.7%	14.0%	4.0%	2.2%	14.8%	21.1%	25.4%	6.2%	4.7%	7.1%	8.6%	6.9%
Cr#	64.4%	63.9%	63.5%	58.8%	66.8%	64.6%	69.9%	65.7%	71.0%	65.6%	59.4%	66.6%	65.0%	58.6%	66.8%	62.1%	64.6%	62.8%	67.6%	70.7%	70.7%	62.0%	67.4%	65.7%	64.0%

Kapalagulu (Kap.) samples: KP01 = KPD066-65.1m; KP02 = KPD066-149.7m; KP03 = 166.7m; KP04 = KPD066-488.1m; KP05 = KPD066-662.1m.
Musongati (Mus.) samples: MS01 = MUS-F059-246m; MS02 = MUS-F059-438m; MS03 = MUS-F060-157m; MS04 = MUS-F060-295m.

4. Comparative Petrology of the KMKA intrusions

To evaluate the possible igneous processes that have led to contrasting major oxide compositions of chrome-spinel grains of the various KMKA intrusions, a petrological study (petrographic examination and whole-rock geochemical analysis) of fine-grained aphyric peripheral sill and marginal rocks has been carried out. These samples do not necessarily contain chromite grains, but on textural grounds are thought to be representative of basaltic liquids derived from the primitive melts from which the bulk of the cumulate rocks crystallized. They can therefore inform us about processes such as fractional crystallization and assimilation-contamination. This work is an extension of previously published work (Evans, 1999; Evans et al., 2000) and newly-derived petrological and geochemical data are presented in Electronic supplementary material Tables S1 and S2. The results are briefly summarized here and incorporated into the discussion below.

4.1. Kabanga

Previous petrological studies detailed above and the present work indicate that the peripheral sills and marginal rocks at Kabanga are noritic and have the composition of siliceous high-magnesian basalts or silica-oversaturated magnesian tholeiites, with both quartz and orthopyroxene present in the mode and clinopyroxene a relatively minor component (electronic supplementary material Table S1). The early and voluminous crystallization of orthopyroxene and suppression of clinopyroxene and plagioclase in these rocks is due to the high SiO_2 and relatively lower CaO content than is normal in tholeiitic basaltic liquids, likely due to bulk incorporation of abundant crustal material. Modelling the crystallization sequence of a melt with the composition of these samples, using the PELE program of Boudreau (1999) indicates that they would crystallize spinel and olivine first followed by orthopyroxene and then plagioclase, which fits the observed petrographic relations (electronic supplementary material Table S1).

The incompatible trace elements, plotted in a mantle-normalized diagram (Fig. 4a), show that the marginal norites and sills at Kabanga are unusually enriched in large-ion lithophile elements with $(Th/Yb)_N = 5$. However, Nb, Sr, P and Ti show depletions relative to adjacent incompatible elements, which is typical of a crustal signature. Of note is the consistent and distinctive Ba-depleted pattern of highly-incompatible elements relative to Rb and Th, which matches that in the enclosing metasedimentary rocks, and is typical of Proterozoic shales in general (Fig. 4a).

4.2. Kapalagulu

Only one sample of fine-grained equigranular marginal gabbronorite has been found at Kapalagulu that shows petrographic evidence of having crystallized from a crystal-poor magma (randomly-oriented and non-poikilitic fabric). This sample contains dominant fine-grained plagioclase, with lesser orthopyroxene and clinopyroxene, with the latter being more abundant than in the marginal and sill samples from Kabanga. Analysis of major oxides shows a lower MgO content relative to the marginal rocks at Kabanga (electronic supplementary material Table S1), whereas SiO_2 is lower and CaO is more abundant relative to MgO in this sample, consistent with its higher content of plagioclase and clinopyroxene. PELE modelling shows that a melt of this composition would crystallize olivine followed by plagioclase, and then clinopyroxene. Orthopyroxene would start to crystallize relatively late in the sequence for this sample (electronic supplementary material Table S1).

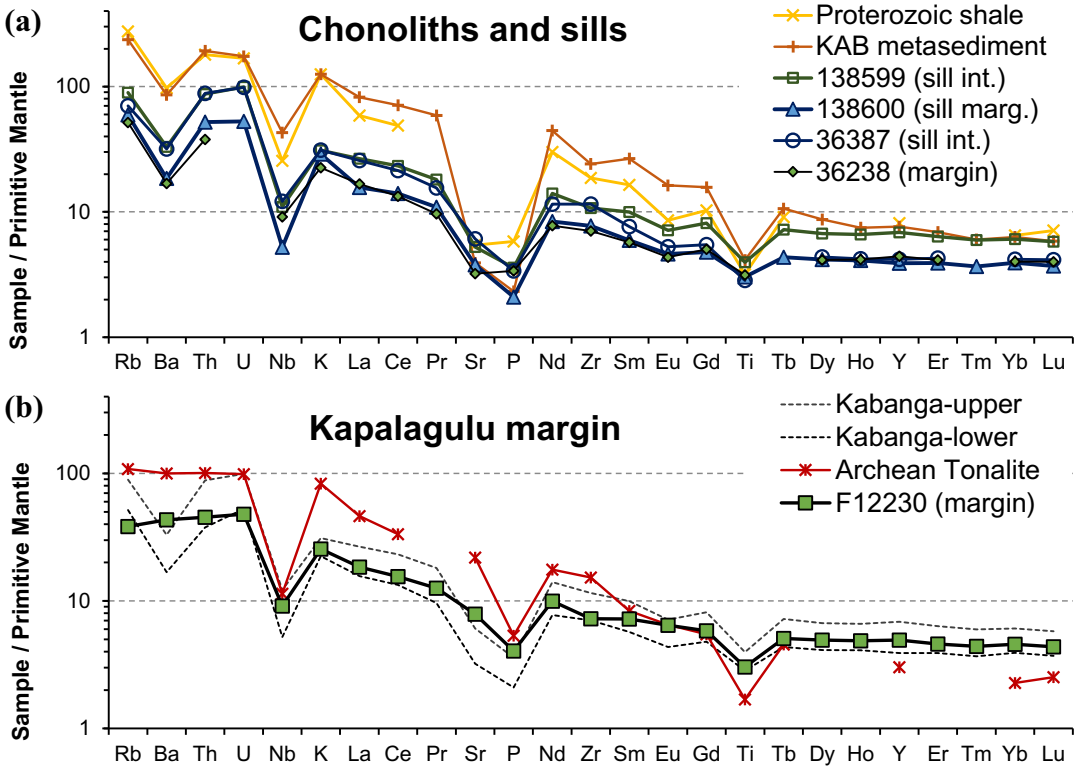

Fig. 4. Mantle-normalized diagrams of incompatible trace elements in samples representing liquid compositions from the margin of KMK intrusions or adjacent sills and their possible contaminants: **a)** Kabanga area ("sill int." refers to samples from the differentiated interior of peripheral sills; "sill marg." refers to the samples from the chilled margin of the sill; "KAB metasediment" is the average of 4 analyses of metasiltstone and metapelite from the Kabanga and Luhuma areas); **b)** Kapalagulu area. Proterozoic shale and Archæan tonalite values are from Condie (1993) and primitive mantle (pyrolite) values are from McDonough and Sun (1995).

The sample's pattern on a mantle-normalized trace-element diagram is very like that of the marginal rocks at Kabanga (Fig. 4b). There is the same enrichment of highly-incompatible elements and the flat pattern in the middle and heavy rare-earth elements. A notable difference is the lack of a strongly negative Ba anomaly, which is such a characteristic feature of the sills and marginal rocks at Kabanga. This may be an indication of a distinct Archæan tonalite-trondhjemite contamination signature at Kapalagulu (Fig. 4b).

5. Composition of chromites of the KMKA intrusions

5.1. Major oxide variations

Chromite is ubiquitous in the samples of orthocumulate and mesocumulate textured peridotite and olivine norite from the intrusions, and takes the form of small to medium (30–200 μm), euhedral grains (type A1 – most abundant; e.g. Fig. 3a–d), or larger (150 to 500 μm), anhedral interstitial grains (type A2 – less abundant; e.g. Fig. 3e, f). Texturally, the chromite grains are mostly situated within poikilitic or interstitial (post-cumulus) grains of plagioclase, phlogopite, clinopyroxene, orthopyroxene and sulphide (Fig. 3b, c, e). They also occur more rarely as small, rounded grains within cumulus olivine and as euhedral grains within cumulus orthopyroxene (Fig. 3a, d). Chromite is more abundant in the olivine-rich cumulate rocks of the Kapalagulu intrusion (locally forming near-massive chromitite seams of 0.001–0.1 m thickness) compared to those of the Kabanga, Muremera and Musongati intrusions.

Analysis of major oxides in chromite and in host silicates by EPMA shows that there is a positive correlation between Mg/(Mg + Fe^{2+}) ratios in chromite and its host silicate mineral in all the intrusions, particularly for olivine (Fig. 5a). There is more scatter in the plot for pyroxenes (Fig. 5b) than for olivine. The Mg/(Mg + Fe^{2+}) ratio of chromite enclosed in pyroxene tends to be higher than that enclosed in olivine. In both cases, the range of values of this ratio is similar to that seen in equivalent rock types of the Great Dyke (Fig. 5).

The major oxides of the chromites (Tables 1 and 2 and Supplementary material Table S4) show normal compositional trends relative to the field of layered intrusions in the world-wide compilation of Barnes and Roeder (2001; Fig. 6). There is a wide spread of Mg# (Mg/[Mg + Fe^{2+}] atomic ratio in percent) between 15 and 60%, while the Cr# (Cr/[Cr + Al] atomic ratio in percent) has a relatively narrow range of 60–75%, both of which are considered normal for orthocumulate rocks in tholeiitic layered intrusions (Fig. 6b). Of note, however, is the negative correlation of

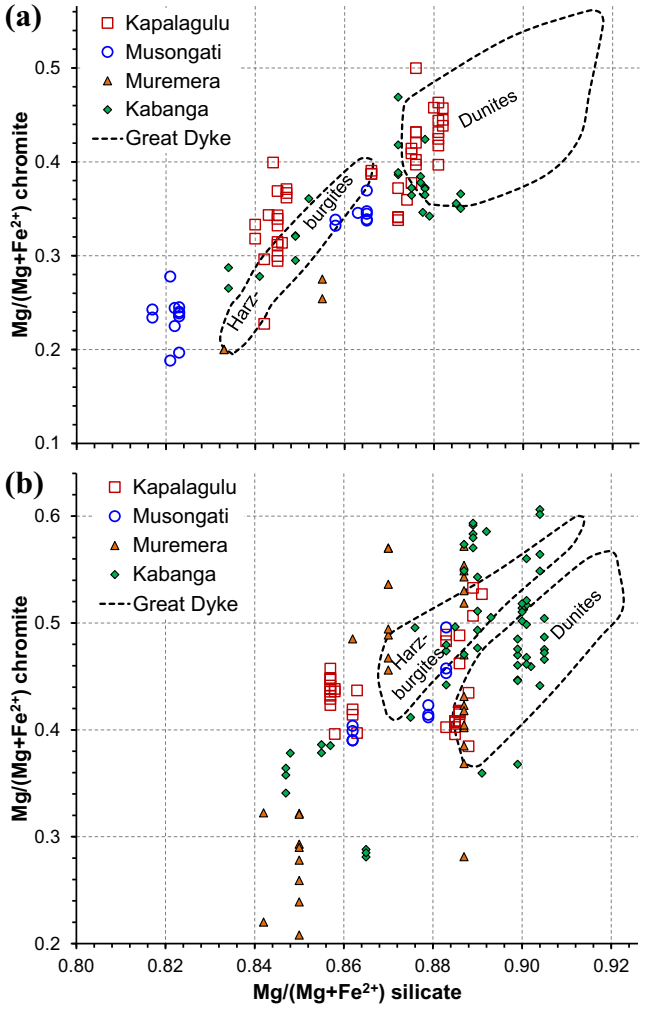

Fig. 5. Relationship of Mg / (Mg + Fe^{2+}) molar ratios of chromite with their enclosing ferromagnesian silicate minerals in the KMKA intrusions: **a)** chromite in olivine; **b)** chromite in orthopyroxene. Fields outlined by dotted line are those for harzburgites (ortho-, mesocumulates) and dunites (adcumulates) of the Ultramafic Section of the Great Dyke (Wilson, 1982).

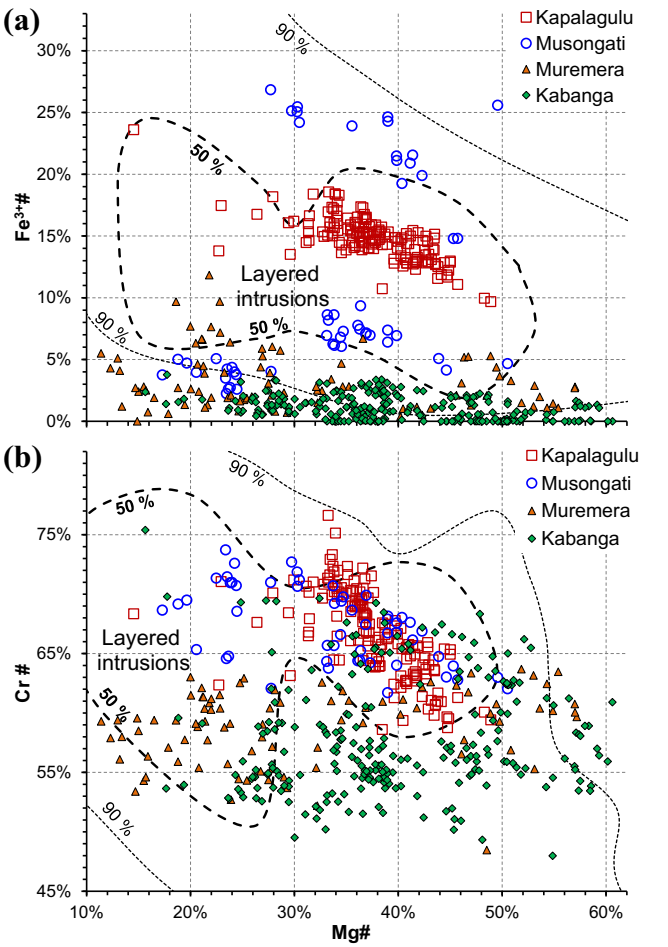

Fig. 6. Compositional variation of major element molar ratios of chromites in the KMKA intrusions: **a)** Fe^{3+}# vs. Mg#; **b)** Cr# vs. Mg#. Dashed lines indicate the 90 percent and 50 percent fields of chrome-spinels in layered intrusions (excluding chromitite seams) from the compilation by Barnes and Roeder (2001).

Mg# with Cr# for the Kapalagulu chromites, in contrast to the relatively flat or indistinctly scattered range for those of the Kabanga and Muremera intrusions. Many chromites from Kabanga also have comparatively low values of Cr#, between 50 and 57%.

A stronger contrast between the chromites of the different intrusions is seen in the diagrams involving Fe^{3+} (Figs. 6a, 7a). Chromite from the Muremera, Kabanga and parts of the Musongati intrusions differ markedly from most layered intrusion chromites in having low values of Fe^{3+}#, whereas those from Kapalagulu have normal levels. Most chromites from the Kabanga and Muremera chonoliths have low to extremely low values of Fe^{3+} (in some cases the stoichiometric recalculation results in negative values due to imprecision of the other major oxides, particularly Ti, and these have been set at zero). Remarkably, even the more Fe^{2+}-enriched chonolith-hosted chromites (with Mg# < 30%) still have very low Fe^{3+} contents (Fig. 6a). The chromites from three samples of the Musongati intrusion also have quite low Fe^{3+}# values, but a fourth sample plots within the usual field of layered intrusions, indicating highly variable conditions in this intrusion. The Kapalagulu chromites have consistently higher levels of Fe^{3+}# that plot entirely within the 50% field of layered intrusions (Table 2; Fig. 6a).

5.2. Minor oxide variations

Of the minor oxides, TiO_2, MnO and ZnO tend to be enriched together with Fe^{2+} and with Fe^{3+} at the expense of MgO and Al_2O_3, during reaction of chromite with evolved late interstitial liquids and during subsolidus equilibration with olivine. TiO_2 is particularly sensitive as an indicator of reaction with late liquids (Roeder and Campbell, 1985), as can be seen in Fig. 7a, in which

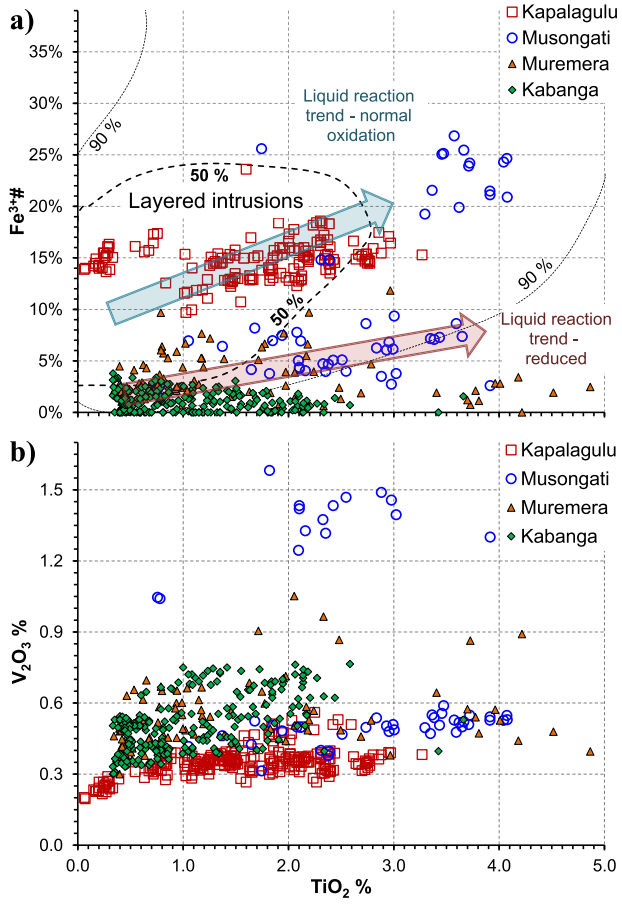

Fig. 7. Variation of liquid reaction indices of chrome-spinels in the KMKA intrusions: **a)** Fe^{3+}# vs. TiO_2; **b)** V_2O_3 vs. TiO_2. Dashed lines in (a) indicate the 90 percent and 50 percent fields of chrome-spinels in layered intrusions (excluding chromitite seams) from the compilation by Barnes and Roeder (2001).

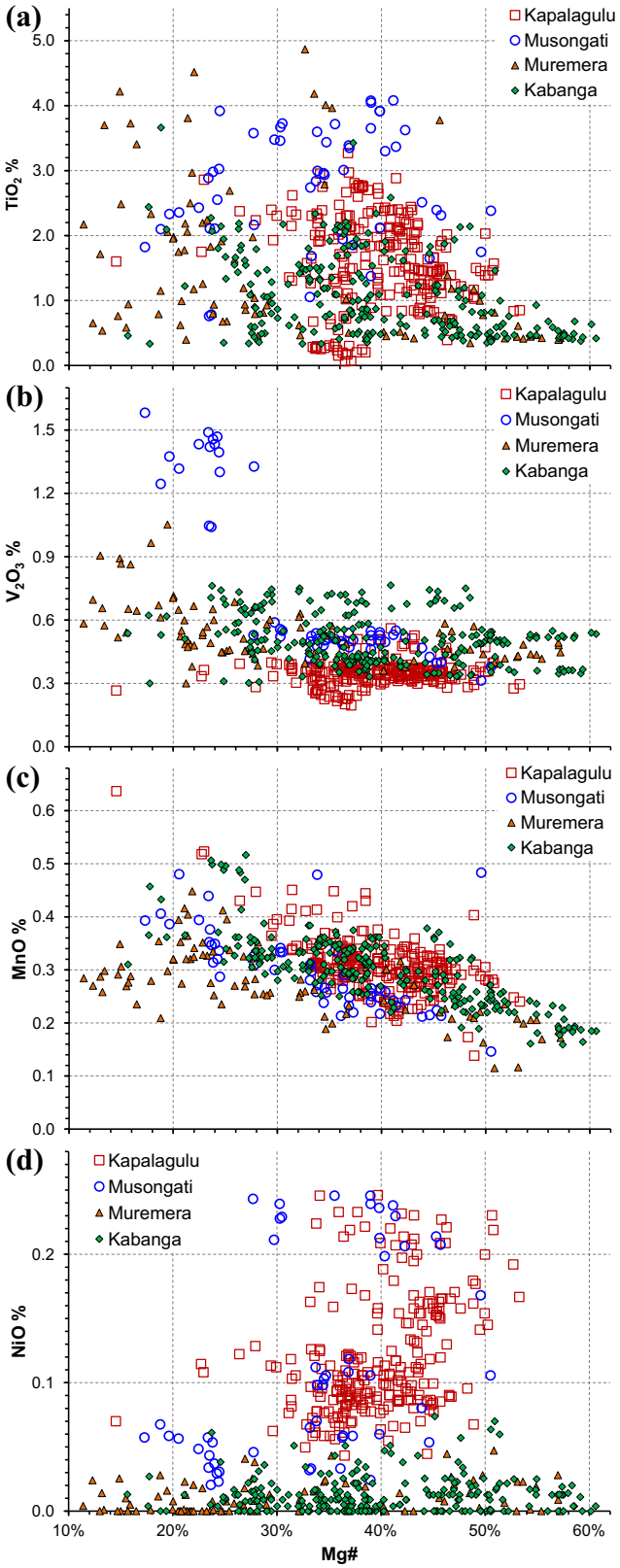

Fig. 8. Compositional variation of minor elements (weight%) of chrome-spinels in the KMKA intrusions: **a)** TiO_2 vs. Mg#; **b)** V_2O_3 vs. Mg#; **c)** MnO vs. Mg#; **d)** NiO vs. Mg#.

TiO_2 and Fe^{3+}# are positively correlated for the layered intrusion samples. The chromites of the Kapalagulu intrusion follow a "normal" liquid reaction trend, plotting through the middle of the 50% field of global layered intrusion chromites, whereas the Musongati chromites follow a positive correlation trend with distinctly lower values of Fe^{3+}#. The chonolith-hosted chromites of Kabanga and Muremera follow a flat liquid reaction trend with hardly any variation of Fe^{3+}# with increasing TiO_2 content. There is a complete overlap in the range of values of MnO and ZnO in chromites for all the KMKA intrusions and they are positively correlated with Fe^{2+} (Figs. 8c). The good inverse correlation between MnO and Mg# is an indication that the chromites analysed have not suffered significant alteration (Barnes, 2000).

The levels of V_2O_3 in the chromites are relatively restricted between about 0.3% and 0.8%, and show a weak or negligible correlation with Fe^{2+} and Fe^{3+} (Fig. 8b). As is the case for Fe^{3+}# and Cr#, there is a moderate distinction between V_2O_3 levels in Kapalagulu chromites and those of the other intrusions, this time with the Kapalagulu chromites having the lowest V_2O_3. Two samples, one from Musongati (MUS-F059-246.8m) and one from Muremera (MURB_D002-227m) have chromite with much higher levels of V_2O_3, between 0.9 and 1.5% at low levels of Mg#. There is a very weak correlation between TiO_2 and V_2O_3. (Fig. 7b), showing that V is not significantly enriched by reaction with late residual liquid, and that the correction for X-ray peak overlap between Ti and V has been successful.

The levels of NiO in the chromite of the lopolithic layered intrusions are moderate, with highest levels in the more Mg-rich chromites of the Kapalagulu and Musongati intrusions (Table 2; Fig. 8d) and this is the case also for the olivine in these layered intrusions (Fig. 9). The most Mg-rich olivines from Kapalagulu, which come from the basal adcumulate dunites of the Lubalisi section, are comparable in NiO content with olivines of the unmineralized Vaigat formation picrite lavas from West Greenland (Fig. 9). However, in many chromites from the chonoliths (Kabanga and Muremera), NiO is so low as to be below detection limits for the method (<0.03 wt%; Fig. 8d). This may in part be explained by the very low Fe^{3+} content of these chromites, as it is well known that Ni has a strong preference for the octahedral site in the inverse spinel structure (Barnes and Tang, 1999). However, as the NiO content of coexisting olivines in the chonolith samples is also low (Fig. 9), this seems to be a genuine geochemical depletion feature of the magmatic system.

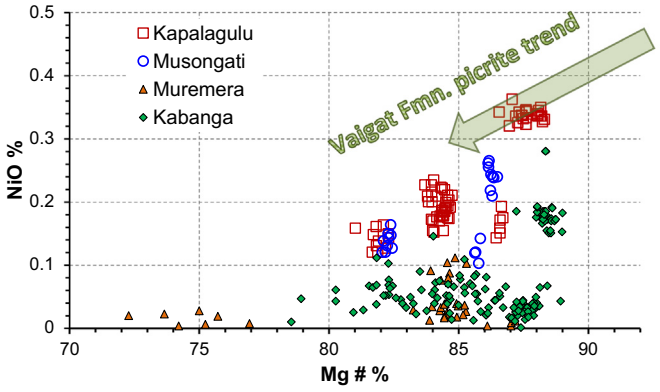

Fig. 9. NiO content versus Mg# (forsterite content) of olivine in the KMKA intrusions. Analysis by wavelength dispersive EPMA undertaken at the same time as and using similar conditions to the analysis of chrome-spinels described above. The Vaigat Fmn. picrite trend shows the composition of olivines from the Vaigat Formation of West Greenland (Larsen and Pedersen, 2000).

6. Discussion

6.1. Possible magma contaminants

Maier et al. (2008, 2010) have already shown based on whole-rock trace element and stable (O, S) isotope measurements that all the KMKA intrusions, including the Kapalagulu intrusion, have undergone contamination by crustal material to varying extents. For the Kabanga and Musongati intrusions, they identified this crustal material as being dominantly sedimentary host rocks of the KAB. The whole-rock analyses of fine-grained marginal and sill rocks from Kabanga in this study also show a strong sedimentary rock signature in their trace-element patterns.

Furthermore, the evidence of crystallization of chromite from a strongly reduced magma seen in the cumulate rocks of Kabanga, Muremera and in parts of the Musongati intrusion is a strong and independent argument that this crustal contamination included a significant amount of carbonaceous mudstone. The Kabanga, Muremera and Musongati intrusions have all been emplaced at a similar stratigraphic level within the Ruvubu SF1 unit, which lies above the thick package of carbonaceous schists of the Muyaga SF1 (Fig. 1c). It is therefore quite reasonable to suppose that the magmas supplying the chonoliths and the Musongati lopolith have been significantly modified while traversing the carbonaceous Muyaga SF1.

The Kapalagulu lopolithic intrusion, however, has been emplaced at or just below the unconformable contact between the non-carbonaceous Itiaso Group and the amphibolitic paragneisses of the Wakole Terrane. Its internal crystallization sequence (peridotite-troctolite-gabbronorite) is distinct from the peridotite-orthopyroxenite-norite trend of the Musongati, Muremera and Kabanga intrusions. Its marginal rocks show a possibly distinct contamination character with a much more subdued negative Ba anomaly (Fig. 4). I propose that this indicates that the parental magma of the Kapalagulu intrusion was contaminated by a greater proportion of normally-oxidized infracrustal gneisses of Archæan to Palæoproterozoic age rather than supracrustal sedimentary material.

Such a hypothesis may be tested by comparing the Kapalagulu magma with coeval mafic rocks that have been emplaced within Archæan infracrustal rocks. The dolerite rocks of the Lake Victoria Dyke Swarm (LVDS), which are coeval with the KMKA mineralized intrusions, are located to the east of the KMK alignment (Fig. 1a), and are mostly emplaced into Archæan tonalite-trondhjemite rocks of the Tanzanian craton or into volcano-sedimentary rocks of the Palæoproterozoic Buganda group which overlies this craton in southwestern Uganda (Westerhof et al., 2014). Mäkitie et al. (2014) identify several geochemical groupings within these dykes, which they propose to represent varying degrees of mixing of magmas from an asthenospheric melt source and a variably metasomatized or "contaminated" sub-continental lithospheric mantle source.

In particular, they identify a high $(La/Sm)_N$ geochemical grouping that is mostly emplaced as broad sill-like gabbronorite bodies within the basal part of the KAB sediments, and contrast this with the main group of gabbro dykes emplaced within Archæan crust and Palæoproterozoic cover rocks similar to those of the Wakole Terrane. The sill-like gabbronorite bodies with high $(La/Sm)_N$ values have more siliceous basaltic andesite compositions with lower CaO/Al_2O_3 ratios than the gabbroic dykes, and their chondrite-normalized patterns are similar to those of the marginal rocks of the Kabanga chonoliths (Mäkitie et al., 2014). The two petrological and geochemical groups distinguished within the LVDS have their direct counterpart with the distinction between sediment-contaminated marginal rocks of the chonoliths and the gneiss/

tonalite-contaminated marginal rock from Kapalagulu. These geochemical distinctions can very well be explained by contamination of a primitive asthenospheric melt by different types of continental crust, with the main group contaminated by deeper (reworked) Archæan granitoidal crust and the high $(La/Sm)_N$ group contaminated by KAB or other sedimentary rock, as Maier et al. (2010) have demonstrated.

6.2. Chromite-liquid reaction and oxidation state

The correlation between Mg# values of chromite and its host ferromagnesian silicate, and the relatively low values of Mg# ratio for the chromites in olivine in orthocumulates (Fig. 5a) suggests that both olivine and chromite reacted with evolved interstitial liquid, as in many other slowly-cooled intrusions such as the Great Dyke (Wilson, 1982). The greater scatter in the plot for pyroxenes (Fig. 5b) is possibly due to variably effective armouring of early-crystallized chromites from reaction with liquid (Roeder and Campbell, 1985). The pattern of a wide spread of Mg# values for a limited variation of Cr# in chromite (Fig. 6b) and enrichments in TiO_2 (Fig. 8a) are also attributed to this continual reaction of the early-formed spinel with nearby interstitial liquid and subsequent subsolidus equilibration with enclosing ferromagnesian minerals (olivine, pyroxene) in these slowly-cooled layered intrusions (Roeder and Campbell, 1985; Barnes and Roeder, 2001).

The present work shows that the chromites that are present in the ultramafic cumulates of the Kabanga-Muremera-Musongati intrusions have crystallized from or at least equilibrated with a variably reduced melt. The chromites from the chonolithic intrusions have particularly low $Fe^{3+}/\Sigma Fe$, even in MgO-poor, TiO_2-rich chromites hosted within late interstitial minerals, which are thought to have reacted most with evolved interstitial melt (Fig. 7a). The olivine-orthopyroxene-spinel oxy-barometer of O'Neill and Wall (1987) should be able to indicate the relative fO_2 of the melt based on the $Fe^{3+}/\Sigma Fe$ in the chromite.

This oxy-barometer can be applied to chromites of the Kapalagulu and to some samples of the Musongati intrusion as these samples are relatively unaltered and the calculation of Fe^{3+} by stoichiometry is relatively precise and has been controlled by secondary standards. These samples, with higher levels of calculated Fe^{3+}, give results for fO_2 of between +0 and +1 log units relative to the quartz-magnetite-fayalite (QFM) buffer. However, quantitative application of this oxy-barometer to the low-Fe^{3+} chromites of the chonoliths is not possible due to the large relative errors in the stoichiometric estimation of Fe^{3+} in the chromite and the ubiquitous partial serpentinization of olivine, meaning it is very rare to find all three minerals in demonstrable equilibrium. The qualitative application of the oxy-barometer indicates much lower values of fO_2 of the melt in the chonoliths, based on the lower, but imprecise values of Fe^{3+} in the chromites and on the similar range of compositions for olivine and orthopyroxene as found in the Kapalagulu intrusion.

The low fO_2 of the chonolith systems is independently backed up by the higher levels of V in their chromites compared to those of the Kapalagulu intrusion (Figs. 7b, 8b). Papike et al. (2004) have used the V content of chrome-spinels to show that basaltic melts on Earth, Mars and the moon have distinctive oxidation states, with those of the Earth being more oxidized than those of the moon. They base their findings on the experimental work of Canil (1999), which has been updated by Mallman and O'Neill (2009), determining the partition coefficients of V in its various cationic valence states between spinel and melt. Essentially, the partition coefficient of V^{3+} into spinel is an order of magnitude higher than that of V^{4+}. At the moderately oxidized conditions that are found in Earth's magmatic systems, V^{4+} is the dominant species, whereas at the more reducing conditions such as are found in lunar magmatism, the V^{3+} ion is dominant and lunar basalts have correspondingly more V-rich chromites than Earth's. The higher V_2O_3 content of chromites from the Kabanga, Muremera and parts of the Musongati intrusions shows that they have crystallized from or equilibrated with a more reduced magma than that of Kapalagulu.

The mafic-ultramafic rocks of the Kabanga-Muremera-Musongati intrusions are all intruded into the sulphide-bearing Ruvubu SF1 Superformation (Fig. 1a, c). This is a pelitic to semipelitic unit containing abundant thin laminæ of iron sulphides in layers near its base (Fig. 2a), but relatively little carbonaceous material. The barren sulphides in these schists (mostly monoclinic pyrrhotite and lesser pyrite) have distinctive strongly positive $\delta^{34}S$ isotopic ratios, suggesting they were derived by seawater sulphate reduction by bacteria in a closed hypoxic basin (Maier et al., 2010). It is the equally positive $\delta^{34}S$ isotopic ratios (+16 to +25‰) of the nickel sulphide mineralization at Kabanga that led Maier et al. (2010) to postulate that the bulk of the S in the Kabanga Ni deposits was derived by bulk assimilation of sulphidic sediment and reaction of the resulting sulphide xenomelt with chalcophile elements in the magma in a complex and long-lived flow-through magma system.

The low Fe^{3+} and higher V_2O_3 contents of chromite from the chonolithic intrusions are equally distinct signals of the strongly reduced nature of the magma. The most obvious candidate for reduction of this kind, below the normal range for mantle melts, would be the extensive carbonaceous sediments that occur in the Muyaga SF1 Superformation below the intrusions (Figs. 1c, 2a). I propose that a significant part of the sediment contamination that led to not only the reduction of the magma, but also the production of abundant sulphide xenomelts that were part of the mineralizing process, occurred while the parental magma was resident in a magma chamber, or was passing through conduits, within this sulphidic and carbonaceous Muyaga SF1 Superformation. This implies that the magma was already saturated with sulphur and laden with immiscible sulphide droplets before it arrived in its emplacement position in the Ruvubu SF1 Superformation. This hypothesis is in accord with that already proposed by Maier et al. (2010), but can be tested further by analysing the sedimentary sulphides of the Muyaga SF1 Superformation for S isotopes to compare them with the already measured values of the nickel sulphide deposits. All samples of sulphidic sedimentary rock that have so far been analysed for S isotopes in the KMKA belt have come from the sediments of the Ruvubu SF1 Superformation adjacent to the intrusions, which may not necessarily have contributed much material to the nickel sulphide deposits.

6.3. Relative timing and processes of contamination, sulphide liquation, fractional crystallization and emplacement

As well as having contrasting levels of Fe^{3+} and of V in their chromites, the Kapalagulu and Kabanga intrusions also have differing levels of Ni in both their olivine and chromite. The Kabanga and Muremera chromites are strongly depleted in Ni relative to those of Kapalagulu. This is the case for all chromites of these intrusions, irrespective of whether they are contained within or are adjacent to sulphide aggregates, thus subliquidus or subsolidus equilibration of the chromite with adjacent sulphide (as proposed by Barnes and Tang, 1999) is not the only factor involved in this depletion. This feature can be explained in two ways: either the Kabanga and Muremera magmas reached sulphur saturation earlier than crystallization of chromite and olivine or they have experienced a simultaneous sulphur saturation and olivine-chromite crystallization with a low R-factor (Campbell and Naldrett, 1979). In the first case, early sulphur saturation of the magma at a deeper level would have formed an immiscible sulphide melt that

collected much of the magma's chalcophile elements prior to crystallization of the chromites and olivine, thus depleting this magma. However, early and deep sulphur saturation, without the involvement of large amounts of sedimentary sulphide would only produce small quantities of immiscible sulphide relative to the volume of silicate melt (high R factors) and there may not be enough sulphide to deplete the magma so thoroughly as is observed.

In the second scenario, a later and shallow sulphur saturation caused by massive assimilation of sedimentary sulphides, as was proposed by Maier et al. (2010) would lead to formation of a much larger volume of sulphide melt (lower R factor). An efficient extraction of Ni and the other chalcophile elements into the sulphide melt could take place in the chonolith, so long as this sulphide melt was thoroughly mixed with the magma by turbulent flow. This should be a more effective mechanism to explain the very depleted levels of Ni in olivine and chromite of the chonolithic intrusions.

Significant assimilation of nearby sulphur-bearing sedimentary material into the chonoliths is indicated by the sulphur isotope values of the mineralization and by the reduced condition of the magma deduced from the chromite compositions. Such a mechanism implies that olivine and chromite crystallization mostly occurred during or after the major sediment assimilation, which is proposed above to have taken place while the magma was traversing the Muyaga SF1 Superformation. No dyke-like feeder has been identified at Kabanga despite intense drilling. Based on the observed predominance of near-concordant sill-like intrusion of minor intrusive bodies related to the main chonoliths at Kabanga and Muremera, it is expected that the magma supplying the chonolith has travelled largely horizontally with only minor local transgressive steps up through the stratigraphy. This implies that the assimilation of carbonaceous sediments of the Muyaga SF1 may have occurred some distance away from the final site of deposition and solidification of the sulphides.

The chonoliths themselves are most likely not the product of a single pulse of magma. Maier et al. (2010) speculate that they have been the locus for repeated flows of magma of varying levels of Ni depletion and carrying more or less sulphides. There may have been reverse-flow or backward cascading of denser liquid sulphides along flow pathways once the main flow pulse had waned (Saumur et al., 2015). There could also have been flow of later pulses of less contaminated and less depleted magma over the top of or through stagnant early-formed sulphides, upgrading their tenors and changing the geochemical characteristics of associated olivine and chromite. The final arrangement that we observe now is the result of the integration of all these processes; the richest sulphide deposits are likely to show the greatest complexity in the geochemical characteristics of their associated silicates and chromites.

6.4. Application to exploration of the East African nickel belt

Exploration for nickel sulphides within the belt has in the past relied heavily on airborne geophysical techniques to penetrate below the thick lateritic soils that cover much of the area and particularly to target the electrically conductive massive sulphides (Wolfgram and Golden, 2001; Evans et al., 2016). However, the signals from such remote sensing techniques do not discriminate very well between genuine nickel sulphide-bearing rocks and other strongly magnetic and conductive rocks such as the carbonaceous pyrrhotite-bearing sedimentary host rocks. Ground verification is required to screen the spurious electromagnetic anomalies and to provide a priority ranking of the remaining anomalies before undertaking the expensive task of drill testing. I propose that one of the techniques that could be useful for this ground work is the collection of heavy mineral concentrates from drainage courses and the identification and analysis of their oxide minerals.

Chromite is virtually restricted to ultramafic rocks and is thus a rare mineral in the continental crustal setting. It is also relatively resistant to surface weathering and oxidation compared to the sulphides and silicates that surround it in ultramafic rock. It should be found not only in surficial weathered ultramafic rock, but also in stream and river drainages, especially in trap sites where water flow changes from the turbulent to the laminar regime. In the East African Nickel Belt, chromite has been found largely intact within lateritic rocks (Bandyayera, 1997), in sulphidic gossans and in the streams draining from them (Evans and Ntungwanayo, 2014). In exploration for nickel sulphides it may thus be used as an indicator mineral to confirm the presence of ultramafic rock.

Not only does the presence and comparative abundance of chromites in a sample confirm the location of ultramafic rock within the drainage area, but analysis of the chromites can provide very useful information on the history of sulphur saturation, contamination and emplacement of the intrusive rocks. Only one or two well-positioned bulk sediment samples of 10–20 kg may be needed from each airborne anomaly site to test the anomalies in this way. The bulk sample would have to be concentrated by gravity methods, either at the site or at a suitable laboratory, where further concentration of certain grain size ranges (normally 0.1–0.5 mm) and grain identification and sorting can be carried out (Averill, 2011). The cost of such a follow-up technique is thought to be reasonable with respect to the cost of the airborne geophysical surveys and of the subsequent drilling campaign to test the anomalies.

Suitably experienced mineral counters can visually identify and count chromite grains within a representative stream sediment concentrate (Averill and Huneault, 2016), as well as note additional features such as size and external texture or shape of the grains. If the abundance of chromite grains recovered from a sample is sufficient (>100 for example), they can be mounted in epoxy resin and polished for further petrological analysis. For instance, the presence or absence of internal zoning can be seen microscopically, and rapid analyses of major oxides made by scanning electron microscope equipped with an energy dispersive spectrometer. Such rapid analyses can determine basic elemental ratios such as Mg#, Cr# and Fe^{3+}#, which may be sufficient for first-pass characterization of samples containing abundant chromite. These element ratios will indicate the cooling history (wide spread of Mg# and Fe^{3+}# values indicating reaction with interstitial liquid, for example), and potential type of contamination (carbonaceous sediments shown by a low Fe^{3+}# range, other contaminants shown by higher Fe^{3+}# trends; Fig. 10a). Further information on the oxidation state of the magma (V_2O_3 values) and on the interaction of the chromite with magmatic sulphides (depletion of NiO) would need higher quality analysis by wavelength-dispersive EPMA. Even more information could potentially be extracted by analysis of trace elements in the chromite by laser-ablation coupled to ICP-MS analysis (Dare et al., 2014; Pagé et al., 2012), but this would require very thorough studies before the significance of any element variation could be applied to exploration.

The Harker plots of Fe^{3+}# versus V_2O_3 and of NiO versus V_2O_3 in Fig. 10 are proposed as effective discrimination plots for chromite compositional data obtained in this way. It should be noted that, although the data presented here are discriminated readily into chromite grains derived from reduced versus oxidized magma and chalcophile element depleted versus undepleted magmas, the most prospective anomalies would present mixed populations of chromites representing a variety of magmatic and mineralizing processes. This would indicate a longer-lived system with higher complexity, which as discussed above, should be more favourable for generating economic sulphide mineralization. These particular

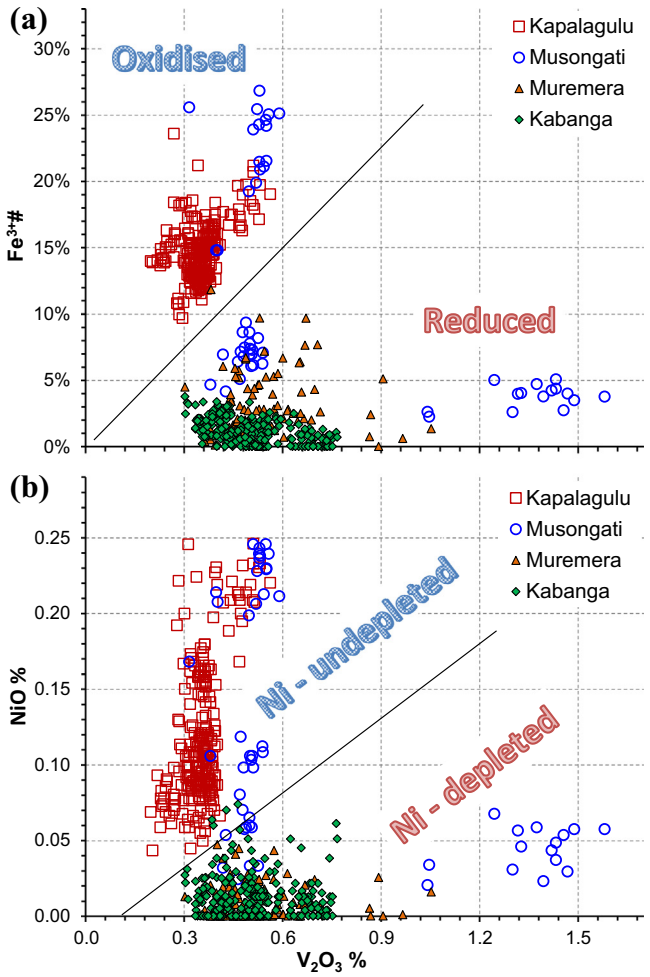

Fig. 10. Proposed discrimination diagrams for chrome-spinels of the KMKA intrusions: **a)** Fe^{3+}# vs. V_2O_3; **b)** NiO vs. V_2O_3.

diagrams may be less effective in other regions or exploration belts and further orientation studies would be needed. It should also be noted that a real stream sediment concentrate sample will contain a much wider variety of chromites, including those that have been subject to greenschist facies alteration, so more scatter on the diagrams could be expected. Filtering of the altered grains prior to analysis would be based on their visible internal zoning and inclusions.

Nevertheless, sampling and analysing for chromite before commencing the drilling of geophysical or geochemical anomalies has the potential to enable a much better understanding of the magmatic and metallogenetic processes that operated within individual intrusions or parts of intrusions. This will help enormously in prioritising anomalies for drilling and should ultimately save money in drilling costs. It is recommended that orientation surveys on chromite populations of stream sediments draining from each of the intrusions studied here should be undertaken before using the technique on untested anomalies in the East African nickel belt.

The proposed technique does of course rely on the exposure of the mafic-ultramafic rocks at the surface such that the cumulate chromite grains will weather out and be released into the drainage system. There will be cases where the geophysical techniques can detect an ultramafic body at depth, but it will not be detected by any surface observation or sampling technique because it is completely enclosed within the host rocks without outcropping (a "blind" intrusion or deposit). In this case, the pre-drilling investigation may need to include other surface methods such as high-sensitivity soil gas or partial leach techniques (after suitable orientation studies have been made) that can detect trace amounts of diagnostic metals directly above deeply buried mineralization (Mann et al., 1998).

7. Conclusions

Analysis of fine-grained marginal rocks from the intrusions of the KMK alignment indicate that they represent contaminated siliceous high-Mg basaltic or andesitic magmas, and that there are subtle differences in the crystallization sequence and the trace element patterns between the Kapalagulu intrusion and the chonolithic intrusions that reflect different types of contaminant. There is a pronounced difference in the Fe^{3+} and V contents of the chromite crystallized from these intrusions, which also suggests that they were contaminated by differing types of crustal material, either oxidized or reduced. The Kapalagulu intrusion may have been contaminated by deeper mid-crustal amphibolitic or tonalite-trondhjemite gneisses, whereas the Kabanga, Muremera and to a lesser extent the Musongati intrusions were contaminated by carbonaceous and sulphidic sediments. The particular contamination signal seen in the chonolithic Kabanga and Muremera intrusions has implications for the timing and mechanism of emplacement of their sulphide mineralization and is reflected in the Ni content of the chromites. Collection and analysis of chromites from concentrated sediment samples may offer a relatively cheap and efficient method to screen and prioritize airborne geophysical anomalies before drilling.

Acknowledgements

Tony Wighton and John Spratt at the Natural History Museum, London are thanked for preparation of excellent petrographical samples and assistance with electron microprobe analysis respectively. Drs. Ian Croudace and Andy Milton of the National Oceanographic Centre, University of Southampton, are thanked for careful analyses of whole-rock samples. The author thanks Sisir Mondal for an invitation to present this work at the 2016 Goldschmidt Conference in Yokohama, Japan. Peter Roeder and Steven Barnes carefully read an early draft of the paper and Ria Mukherjee, Chusi Li and an anonymous reviewer are thanked for their careful reading and useful review comments. Samples for this study were collected during commercial exploration work in the 1990s and early 2000s: permission has been given by the commercial entities to carry out the analytical work on these samples. This research did not receive any specific grant from funding agencies in the public, commercial, or not-for-profit sectors.

Appendix A. Supplementary data

Supplementary data associated with this article can be found, in the online version, at http://dx.doi.org/10.1016/j.oregeorev.2017.03.012.

References

Averill, S.A., 2011. Viable indicator minerals in surficial sediments for two major base metal deposit types: Ni-Cu-PGE and porphyry Cu. Geochem. Expl. Environ. Anal. 11, 279–291.

Averill, S.A., Huneault, R.G., 2016. Basic indicator mineral math: Why visual analysis of the entire heavy mineral fraction of large sediment samples is required on indicator mineral exploration programs in glaciated terrains. Explore 172, 1–14.

Bandyayera, D., 1997. Formation des latérites nickélifères et mode de distribution des éléments du groupe du platine dans les profils latéritiques du complexe de Musongati, Burundi Unpublished Ph.D. Thesis. University of Quebec at Chicoutimi, Canada. 440p., Available online, 2016/01/06.

Barnes, S.J., 2000. Chromite in komatiites, II. Modification during greenschist to mid-amphibolite facies metamorphism. J. Petrol. 41, 387–409.
Barnes, S.J., Kunilov, V.Y., 2000. Chrome spinels and Mg-ilmenites from the Noril'sk 1 and Talnakh intrusions and other mafic rocks of the Siberian flood basalt province. Econ. Geol. 95, 1701–1717.
Barnes, S.J., Roeder, P.L., 2001. The range of spinel compositions in terrestrial mafic and ultramafic rocks. J. Petrol. 42, 2279–2302.
Barnes, S.J., Tang, Z.-L., 1999. Chrome spinels from the Jinchuan Ni-Cu sulfide deposit, Gansu Province, People's Republic of China. Econ. Geol. 94, 343–356.
Baudet, D., Hanon, M., Lemonne, E., Theunissen, K., 1988. Lithostratigraphie du domaine sédimentaire de la chaîne Kibarienne au Rwanda. Ann. Soc Géol. Belg. 112, 225–246.
Boniface, N., Schenk, V., Appel, P., 2012. Paleoproterozoic eclogites of MORB-type chemistry and three Proterozoic orogenic cycles in the Ubendian Belt (Tanzania): Evidence from monazite and zircon geochronology, and geochemistry. Precamb. Res. 192–195, 16–33.
Boniface, N., Schenk, V., Appel, P., 2014. Mesoproterozoic high-grade metamorphism in pelitic rocks of the northwestern Ubendian Belt: Implication for the extension of the Kibaran intra-continental basins to Tanzania. Precamb. Res. 249, 215–228.
Boudreau, A.E., 1999. PELE—a version of the MELTS software program for the PC platform. Comput. Geosci. 25, 201–203.
Campbell, I.H., Naldrett, A.J., 1979. The influence of silicate:sulfide ratios on the geochemistry of magmatic sulfides. Econ. Geol. 74, 1503–1505.
Canil, D., 1999. Vanadium partitioning between orthopyroxene, spinel, and silicate melt and the redox states of mantle source regions for primary magmas. Geochim. Cosmochim. Acta 63, 557–572.
Carmichael, I.S.E., 1967. The iron-titanium oxides of salic volcanic rocks and their associated ferromagnesian silicates. Contrib. Mineral. Petrol. 14, 36–64.
Condie, K.C., 1993. Chemical composition and evolution of the upper continental crust: contrasting results from surface samples and shales. Chem. Geol. 104, 1–37.
Daly, M.C., 1988. Crustal shear zones in central Africa: a kinematic approach to Proterozoic tectonics. Episodes 11, 5–11. Available online, 2016/01/06.
Dare, S.A.S., Barnes, S.-J., Beaudoin, G., Méric, J., Boutroy, E., Potvin-Doucet, C., 2014. Trace elements in magnetite as petrogenetic indicators. Miner. Depos. 49, 785–796.
Deblond, A., Tack, L., 1999. Main characteristics and review of mineral resources of the Kabanga-Musongati mafic-ultramafic alignment in Burundi. J. Afr. Earth Sci. 29, 313–328.
Deblond, A., Punzalan, L.E., Boven, A., Tack, L., 2001. The Malagarazi Supergroup of southeast Burundi and its correlative Bukoba Supergroup of northwest Tanzania: Neo- and Mesoproterozoic chronostratigraphic constraints from Ar-Ar ages on mafic intrusive rocks. J. Afr. Earth Sci. 32, 435–449.
Dick, H.J.B., Bullen, T., 1984. Chromian spinel as a petrogenetic indicator in abyssal and alpine-type peridotites and spatially associated lavas. Contrib. Mineral. Petrol. 86, 54–76.
Duchesne, J.-C., Liégeois, J.-P., Deblond, A., Tack, L., 2004. Petrogenesis of the Kabanga-Musongati layered mafic-ultramafic intrusions in Burundi (Kibaran Belt): geochemical, Sr-Nd isotopic constraints and Cr-Ni behaviour. J. Afr. Earth Sci. 39, 133–145.
Evans, D.M., 1999. High magnesium basaltic origin of Kibaran intrusions, Tanzania. In: Hall, R.P. (Ed.), Abstract in Komatiites, Norites, Boninites & Basalts, KNBB Conference Abstract Volume. University of Portsmouth, United Kingdom, pp. 23–24.
Evans, D.M., 2014. Metamorphic modifications of the Muremera mafic-ultramafic intrusions, eastern Burundi, and their effect on chromite compositions. J. Afr. Earth Sci. 101, 19–34.
Evans, D.M., Ntungwanayo, J., 2014. Étude de l'utilisation de chromite détritique à l'exploration de minéralisation sulfurée de Ni-Cu au Muremera, Burundi. In: Poster and Abstract Volume, 24e Réunion des Sciences de la Terre, Pau, France. Société Géologique de France.
Evans, D.M., Byemelwa, L., Gilligan, J., 1999. Variability of magmatic sulphide compositions at the Kabanga nickel prospect, Tanzania. J. Afr. Earth Sci. 29, 329–351.
Evans, D.M., Boadi, I., Byemelwa, L., Gilligan, J.M., Kabete, J., Marcet, P., 2000. Kabanga magmatic nickel sulphide deposits, Tanzania – morphology and geochemistry of associated intrusions. J. Afr. Earth Sci. 30, 651–674.
Evans, D.M., Hunt, J.P.P.M., Simmonds, J.R., 2016. An overview of nickel mineralization in Africa with emphasis on the Mesoproterozoic East African Nickel belt (EANB). Episodes 39 (2), 319–333.
Fernandez-Alonso, M., Cutten, H., de Waele, B., Tack, L., Tahon, A., Baudet, D., Barritt, S.D., 2012. The Mesoproterozoic Karagwe-Ankole Belt (formerly the NE Kibara Belt): the result of prolonged extensional intracratonic basin development punctuated by two short-lived far-field compressional events. Precamb. Res. 216–219, 63–86.
Glencore, 2016. Glencore Resources & Reserves as at 31 December 2015. Downloaded on 06/01/2017 from Glencore website.
Halligan, R., 1963. The proterozoic rocks of Western Tanganyika. In: Bulletin 23, Geological Survey of Tanzania. Ministry of Mines, Energy and Water, Dar Es Salaam.
Ionov, D.A., Wood, B.J., 1992. The oxidation state of the subcontinental mantle: oxygen thermobarometry of mantle xenoliths from central Asia. Contrib. Mineral. Petrol. 111, 179–193.
Irvine, T.N., 1967. Chromian spinel as a petrogenetic indicator. Part 2, petrologic applications. Can. J. Earth Sci. 4, 71–103.
Keays, R.R., Lightfoot, P.C., 2010. Crustal sulfur is required to form magmatic Ni–Cu sulfide deposits: evidence from chalcophile element signatures of Siberian and Deccan Trap basalts. Miner. Deposita 45, 241–257.
Klerkx, J., Liégeois, J.-P., Lavreau, J., Claessens, W., 1987. Crustal evolution of the northern Kibaran Belt, Eastern and Central Africa. In: Kröner, A. (Ed.), Proterozoic Lithospheric Evolution. American Geophysical Union, Washington D. C., pp. 217–233.
Koegelenberg, C., Kisters, A.F.M., Kramers, J.D., Frei, D., 2015. U-Pb detrital zircon and 39Ar–40Ar muscovite ages from the eastern parts of the Karagwe-Ankole Belt: Tracking Paleoproterozoic basin formation and Mesoproterozoic crustal amalgamation along the western margin of the Tanzania Craton. Precamb. Res. 269, 147–161.
Larsen, L.M., Pedersen, A.K., 2000. Processes in high-Mg, high-T magmas: evidence from olivine, chromite and glass in Palæogene picrites from west Greenland. J. Petrol. 41, 1071–1098.
Lenoir, J.L., Liégeois, J.-P., Theunissen, K., Klerkx, J., 1994. The Palæoproterozoic Ubendian shear belt in Tanzania: geochronology and structure. J. Afr. Earth Sci. 19, 169–184.
Maier, W.D., Barnes, S.-J., 2010. The Kabanga Ni sulfide deposits, Tanzania: II. Chalcophile and siderophile element geochemistry. Mineral. Depos. 45, 443–460.
Maier, W.D., Peltonen, P., Livesey, T., 2007. The ages of the Kabanga North and Kapalagulu intrusions, Western Tanzania: a reconnaissance study. Econ. Geol. 102, 147–154.
Maier, W.D., Barnes, S.-J., Bandyayera, D., Livesey, T., Ripley, E., 2008. Early Kibaran rift-related mafic–ultramafic magmatism in western Tanzania and Burundi: Petrogenesis and ore potential of the Kapalagulu and Musongati layered intrusions. Lithos 101, 24–53.
Maier, W.D., Barnes, S.-J., Sarkar, A., Ripley, E., Li, C., Livesey, T., 2010. The Kabanga Ni sulfide deposit, Tanzania: I. Geology, petrography, silicate rock geochemistry, and sulphur and oxygen isotopes. Mineral. Depos. 45, 419–441.
Mäkitie, H., Data, G., Isabirye, E., Mänttäri, I., Huhma, H., Klausen, M.B., Pakkanen, L., Virransalo, P., 2014. Petrology, geochronology and emplacement model of the giant 1.37 Ga arcuate Lake Victoria Dyke Swarm on the margin of a large igneous province in eastern Africa. J. Afr. Earth Sci. 97, 273–297.
Mallmann, G., O'Neill, H.St.C., 2009. The crystal/melt partitioning of V during mantle melting as a function of oxygen fugacity compared with some other elements (Al, P, Ca, Sc, Ti, Cr, Fe, Ga, Y, Zr and Nb). J. Petrol. 50, 1765–1794.
Mann, A.W., Birrell, R.D., Mann, A.T., Humphreys, D.B., Perdix, J.L., 1998. Application of mobile metal ion technique to routine geochemical exploration. J. Geochem. Explor. 61, 87–102.
McConnell, R.B., 1950. Outline of the geology of Ubende and Ufipa. Bulletin Geol. Surv. Tanganyika, 19. 62 pp.
McDonough, W.F., Sun, S.-S., 1995. The composition of the earth. Chem. Geol. 120, 223–253.
Naldrett, A.J., 2004. Magmatic Sulfide Deposits: Geology, Geochemistry and Exploration. Springer-Verlag, Berlin, Heidelberg, ISBN 978-3-662-08444-1. 727 p..
O'Neill, H., St, C., Wall, V.J., 1987. The olivine – orthopyroxene – spinel oxygen geobarometer, the nickel precipitation curve, and the oxygen fugacity of the Earth's upper mantle. J. Petrol. 28, 1169–1191.
Pagé, P., Barnes, S.-J., Bédard, J.H., Zientek, M.L., 2012. In situ determination of Os, Ir, and Ru in chromites formed from komatiite, tholeiite and boninite magmas: Implications for chromite control of Os, Ir and Ru during partial melting and crystal fractionation. Chem. Geol. 302–303, 3–15.
Papike, J.J., Karner, J.M., Shearer, C.K., 2004. Comparative planetary mineralogy: V/(Cr + Al) systematics in chromite as an indicator of relative oxygen fugacity. Am. Mineral. 89, 1557–1560.
Roeder, P.L., Campbell, I.R., 1985. The effect of postcumulus reactions on compositions of chrome-spinels from the Jimberlana Intrusion. J. Petrol. 26, 763–786.
Saumur, B.M., Cruden, A.R., Evans-Lamswood, D., Lightfoot, P.C., 2015. Wall-rock structural controls on the genesis of the Voisey's Bay intrusion and its Ni-Cu-Co magmatic sulfide mineralization (Labrador, Canada). Econ. Geol. 110, 691–711.
Tack, L., 1995. The Neoproterozoic Malagarazi Supergroup of SE Burundi and its equivalent Bukoban System in NW Tanzania: a current review. Royal Museum of Central Africa (Belgium). Ann. Sci. Geol. 101, 121–129.
Tack, L. and Deblond, A., 1990. Intrusive character of the Late Kibaran magmatism in Burundi. International Geological Corelation Project No. 255 Newsletter/Bulletin 3, 81–87.
Tack, L., Liègeois, J.P., Deblond, A., Duchesne, J.C., 1994. Kibaran A-type granitoids and mafic rocks generated by two mantle sources in a late orogenic setting (Burundi). Precamb. Res. 68, 323–356.
Tack, L., Wingate, M.T.D., deWaele, B., Meert, J., Belousova, E., Griffin, B., Tahon, A., Fernandez-Alonso, M., 2010. The 1375Ma "Kibaran event" in Central Africa: prominent emplacement of bimodal magmatism under extensional regime. Precamb. Res. 180, 63–84.
Theunissen K., Lenoir J. L., Liégeois J-P., Delvaux D. and Mruma A., 1992. Empreinte pan-africaine majeure dans le chaîne ubendienne de Tanzanie sud-occidentale: géochronologie U-Pb sur zircon et contexte structural. Compte Rendus Académie Sciences, Paris, 314-II, 1355–1362.
Van Zyl, C., 1959. An outline of the geology of the Kapalagulu Complex, Kungwe bay, Tanganyika Territory, and aspects of the evolution of layering in basic intrusive. Trans. Geol. Soc. S. Afr. 62, 1–31.
Wadsworth, W. J. 1963. The Kapalagulu layered intrusion of Western Tanganyika. Min. Soc. America, Spec. Pap. 1, 108-115. Download available 2016-01-06.

Waleffe, A., 1966. Etude géologique de l'est du Burundi et stratigraphie du Burundien. Musée Royale de l'Afrique Centrale, Tervuren (Belgique), Département Géologie et Minéralogie Rapport Annuel 1965, 69–74.
Westerhof, A.B.P., Härmä, P., Isabirye, E., Katto, E., Koistinen, T., Kuosmanen, E., Lehto, T., Lehtonen, M.I., Mäkitie, H., Manninen, T., Mänttäri, I., Pekkala, Y., Pokki, J., Saalmann, K., Virransalo, P., 2014. Geology and geodynamic development of Uganda with explanation of the 1:1,000,000 scale geological map. In: Geological Survey of Finland Special Paper 55, Espoo, Finland, ISBN 978-952-217-294-5, p. 387. 2 appendices.
Wilhelmij, H.R., Joseph, G., 2004. Stratigraphic location of platinum mineralisation in the Kapalagulu Intrusion of western Tanzania. In: Ashwal, L.D. (Ed.), Abstracts Geoscience Africa 2004, Vol. 2. Geological Society of South Africa, Johannesburg, South Africa. 709–08.
Wilhelmij, H., Cabri, L.J., 2015. Platinum mineralization in the Kapalagulu Intrusion, western Tanzania. Miner. Deposita 51, 343–367.
Wilson, A.H., 1982. The geology of the Great 'Dyke', Zimbabwe: the ultramafic rocks. J. Petrol. 23, 240–292.
Wolfgram, P., Golden, H., 2001. Airborne EM applied to sulphide nickel: examples and analysis. Explor. Geophys. 32, 136–140.
Wood, B.J., Virgo, D., 1989. Upper mantle oxidation state: ferric iron contents of lherzolitic spinels by ^{57}Fe Mössbauer spectroscopy and resultant oxygen fugacities. Geochim. Cosm. Acta 53, 1277–1291.